



## Calhoun: The NPS Institutional Archive DSpace Repository

---

Theses and Dissertations

1. Thesis and Dissertation Collection, all items

---

1973-03

### Internal ballistics of solid fuel ramjets

Boaz, Lowell David

Monterey, California. Naval Postgraduate School

---

<http://hdl.handle.net/10945/16656>

---

*Downloaded from NPS Archive: Calhoun*



<http://www.nps.edu/library>

Calhoun is the Naval Postgraduate School's public access digital repository for research materials and institutional publications created by the NPS community.

Calhoun is named for Professor of Mathematics Guy K. Calhoun, NPS's first appointed -- and published -- scholarly author.

Dudley Knox Library / Naval Postgraduate School  
411 Dyer Road / 1 University Circle  
Monterey, California USA 93943

INTERNAL BALLISTICS OF SOLID FUEL RAMJETS

Lowell David Boaz



# NAVAL POSTGRADUATE SCHOOL

## Monterey, California



# THESIS

INTERNAL BALLISTICS  
OF  
SOLID FUEL RAMJETS

by

Lowell David Boaz

Thesis Advisor:

D. W. Netzer

March 1973

T154799

Approved for public release; distribution unlimited.



Internal Ballistics  
of  
Solid Fuel Ramjets  
  
by  
  
Lowell David Boaz  
Lieutenant, United States Navy  
B.S., United States Naval Academy, 1967

Submitted in partial fulfillment of the  
requirements for the degree of

MASTER OF SCIENCE IN AERONAUTICAL ENGINEERING

from the  
NAVAL POSTGRADUATE SCHOOL  
March 1973



## ABSTRACT

An experimental investigation of the internal ballistics of solid fuel ramjets was conducted in order to determine the regression rate of the fuel as a function of chamber pressure, inlet air temperature, and air flux rate, and to model the flow in solid fuel ramjets which use sudden expansion flameholders at the inlet. In addition, flame stabilization limits were investigated. A computer solution for the non-reacting flow field gave results in good agreement with experiments.

Solid fuel ramjets have an average regression rate of the fuel that closely follows the theoretical expression derived for kinetically controlled hybrid rocket combustion. The inlet step-height-to-motor-diameter ratio is the dominant parameter in determining flame stability limits. However, inlet velocity is also an important parameter.



## TABLE OF CONTENTS

I.	INTRODUCTION -----	8
II.	METHOD OF INVESTIGATION -----	16
III.	DESCRIPTION OF APPARATUS -----	17
	A. COLD FLOW VISUALIZATION MODEL -----	17
	B. HOT FIRING APPARATUS -----	17
	1. Ramjet Motor -----	17
	2. Ignition System -----	20
	3. Nitrogen Purge and Cooling Air System -	20
	4. Air Flow Control -----	20
	5. Data Acquisition System -----	20
	6. Air Feed System -----	21
IV.	EXPERIMENTAL PROCEDURE -----	22
V.	PISTEP II COMPUTER PROGRAM -----	25
VI.	RESULTS AND DISCUSSION -----	29
	A. COLD FLOW EXPERIMENTS -----	29
	B. PISTEP II RESULTS -----	31
	C. PISTEP II WITH WALL MASS ADDITION -----	33
	D. PMM/AIR RAMJET -----	35
VII.	CONCLUSIONS -----	45
VIII.	SUGGESTIONS FOR FUTURE WORK -----	47
	FIGURES -----	48
	APPENDIX A: PROGRAM TO CONTOUR STREAMLINES -----	71
	APPENDIX B: RAMJET DATA REDUCTION -----	77
	APPENDIX C: NON-SUSTAINING TEST DATA -----	88



LIST OF REFERENCES -----	92
INITIAL DISTRIBUTION LIST -----	94
FORM DD 1473 -----	95



LIST OF TABLES

I.	NOMINAL TEST CONDITIONS -----	23
II.	VARIABLE FUNCTIONS -----	26
III.	TURBULENCE CONSTANTS -----	27
IV.	RESULTS OF PISTEP II CALCULATIONS -----	32
V.	PISTEP II WITH WALL MASS ADDITION -----	35
VI.	ERROR ANALYSIS -----	37



## LIST OF FIGURES

1.	COMBUSTION MECHANISMS -----	48
2.	COLD FLOW VISUALIZATION APPARATUS -----	49
3.	SCHEMATIC OF SOLID FUEL RAMJET APPARATUS -----	50
4.	SOLID FUEL RAMJET MOTOR -----	51
5.	RAMJET MOTOR ON TEST STAND -----	52
6.	TEST STAND -----	53
7.	TEST STAND -----	54
8.	RAMJET MOTOR FIRING -----	55
9.	BOUNDARY CONDITIONS FOR PISTEP II -----	56
10.	BOUNDARY CONDITIONS WITH WALL MASS INJECTION -----	57
11.	REATTACHMENT POINT VS. STEP HEIGHT -----	58
12.	REATTACHMENT POINT DATA COMPARISON -----	59
13.	STREAMLINES FOR NON-REACTING FLOW -----	60
14.	STREAMLINES FOR NON-REACTING FLOW -----	61
15.	STREAMLINES FOR NON-REACTING FLOW -----	62
16.	STREAMLINES FOR NON-REACTING FLOW -----	63
17.	STREAMLINES FOR NON-REACTING FLOW -----	64
18.	STREAMLINES FOR NON-REACTING FLOW -----	65
19.	STREAMLINES FOR NON-REACTING FLOW -----	66
20.	STREAMLINES FOR NON-REACTING FLOW -----	67
21.	STREAMLINES FOR NON-REACTING FLOW -----	68
22.	REGRESSION PATTERNS -----	69
23.	EMPIRICAL REGRESSION RATE EQUATION -----	70



ACKNOWLEDGEMENTS

The author wishes to express his appreciation to Associate Professor David W. Netzer of the Department of Aeronautics for his guidance, encouragement, and assistance throughout the project.

Appreciation also goes to Edward Michelson, Patrick J. Hickey, Jr. and Cecil R. Gordon who with the remainder of the technical staff of the Aeronautics Department furnished timely and efficient technical assistance.

This work was sponsored by the Naval Weapons Center, China Lake, California under Work Request 2-3044.



## I. INTRODUCTION

The solid fuel ramjet can be classified as a special case of the hybrid rocket. That is, the fuel is solid and the oxidizer is gaseous (air). The solid fuel ramjet provides many of the advantages of solid fuel rockets without the weight penalty of carrying its own oxidizer. Ease of handling, storability, weight savings, and possibly greatly increased tactical ranges are among its advantages.

A research project is currently being conducted at the Naval Postgraduate School to model the internal ballistics of solid fuel ramjets. Such a model would provide the design engineer with a working tool that would permit performance parameters and operating characteristics to be predicted. The overall goal of the research project is to develop a model that can predict the regression rate of the fuel as a function of operating and configuration variables. Very little experimental data currently exist that can be used to determine the adequacy of a model, thus the model must be developed in steps verifying each step with experimental data. Non-burning tests to determine flow patterns, non-burning tests with wall blowing to determine the effect of wall mass addition on the flow characteristics, and hot firing tests with various inlet geometries are required. This thesis initiates the overall research project objectives.



Information is provided from several areas of study that are pertinent to the internal ballistics of solid fuel ramjets. Specific areas are flow and heat transfer in ducts with a backward facing step, flame stabilization in high speed flows, hybrid rocket combustion, and thermal decomposition of polymers.

Abbott and Kline [Ref. 1] investigated the turbulent flow over backward facing steps using water flow through a two-dimensional channel. It was found that the recirculation zone consisted of a complex pattern involving three distinct regions. Immediately downstream of the step face there is a three-dimensional zone "characterized by one or more vortexes rotating about an axis normal to the vertical wall." This zone is followed by an almost two-dimensional zone of recirculating flow. The area at the flow reattachment point is characterized by a fluctuating three-dimensional flow. It was also found that the location of the reattachment point remained fixed as Reynolds number and/or inlet turbulence intensity varied, and that increasing the step height moved the reattachment point further downstream from the step face.

Krall and Sparrow [Ref. 2] using water flow through an orifice in an electrically heated circular tube found that local heat transfer coefficients in the separated, reattached, and redevelopment regions are several times larger than those for fully developed turbulent pipe flow. They found that



the maximum heat transfer coefficient occurred in the vicinity of the point of flow reattachment.

At low Reynolds numbers based on downstream pipe diameter (10,000 to 50,000) the heat transfer near the reattachment point varied rapidly with Reynolds number. However, at higher Reynolds numbers (70,000 to 130,000) only a weak dependence was noted. They also found that for weaker separations (small step heights,  $h$ ) the reattachment point was well defined but for strong separations (large step heights) the reattachment point was spread out. This transition from a single well-defined reattachment point to the "spread-out" configuration occurred between  $h/D=0.16$  and  $h/D=0.25$ , where  $D$  is the downstream pipe diameter. The reattachment point was located between 1.25 and 2.5 pipe diameters downstream of the initial separation. Increased step height moved the reattachment point slightly downstream. Reynolds number and Prandtl number had no significant effect on the reattachment point location.

The results of Krall and Sparrow are also in general agreement with the results of Abbott and Kline. For small step heights ( $h/D=.17$ ) the two-dimensional and axisymmetric reattachment points are very nearly equal ( $X_r/D$  from 1.0 to 1.25). However, for larger step heights, the reattachment zone spreads out considerably more for the two-dimensional case than for the axisymmetric case.

The ideal hybrid rocket is one in which a gaseous oxidizer flows over a solid fuel. In a hybrid rocket, gas



phase combustion in the form of a diffusion flame takes place in the turbulent boundary layer formed by the oxidizer flow over the solid surface of the fuel. Heat is transported by convection and radiation to the solid surface which causes decomposition of the fuel. The convective heat transport is complicated by the presence of high rates of wall mass addition. Using a heat transfer limited model, regression rates of the fuel are generally proportional to  $G^n$ , where  $G$  is the total gas flux and  $n$  is a constant (typically 0.8).

Experimental data obtained at low chamber pressure and/or high oxidizer mass flux indicate that the regression rate of hybrid grains becomes less dependent on  $G$ , but is directly related to the partial pressure of the oxidizer in the gas phase [Refs. 3 and 4]. Reduced reaction rates at lower pressures broaden the flame zone. Schlieren studies have also shown that the flame zone broadens at low chamber pressures and may broaden enough to undergo transition to a turbulent premixed flame [Ref. 6]. When the oxidizer is diluted, the diffusion flame moves further away from the surface, increases in thickness, and the flame temperature drops [Refs. 3 and 5]. In addition, surface kinetics may be rate controlling under these operating conditions [Ref. 7]. When these conditions exist, the heat transfer limited model does not adequately describe the combustion process.



Hybrid rockets operating at high chamber pressures are adequately described by a heat transfer limited model. Muzzy [Ref. 4] has reviewed the modifications that have been made to the heat transfer limited model to account for gas phase and surface kinetic effects. The modified models [Refs. 6 and 7] predict a dependence of the regression rate on pressure as well as mass flow rate. For a system where radiative heat transfer can be neglected, Muzzy has shown that the regression rate equation in the kinetically dominated region of operation can be expressed as:

$$\dot{r} = C P^{0.5} G^a X^b$$

where C is a constant, P is pressure, G is total mass flux, X is the longitudinal coordinate, a is a constant that varies from 0.3 to 0.4, and b is a constant that varies from -0.1 to -0.2. Another study by Kustov and Rybanin [Ref. 18] has also treated the pressure sensitive regime of operation.

In a solid fuel ramjet the reacting flow has characteristics that are similar to those discussed above. However, two significant differences exist. Solid fuel ramjets would normally operate at lower chamber pressures than hybrid rockets, resulting in significantly greater port velocities. In addition, the oxidizer in this case is air which would correspond to a severely diluted oxidizer in hybrid combustion. These differences require some means of flame stabilization. A series of tests performed at the United Technology Center [Ref. 8] have shown that one means of



sustaining combustion in a solid fuel ramjet is to use a sudden expansion inlet as is used in dump combustors.

Similar results were reported by McCarthy [Ref. 9].

In a high velocity gas stream, where the velocities of the flow are at least an order of magnitude greater than the turbulent flame speeds of the combustion mixtures, flame stabilization is required. Bluff body flame stabilization has been used successfully in turbojet and liquid fuel ramjet combustor design in the past. Typical flame stabilizers have been V-gutters and rods, or the dome of a can-type combustor [Refs. 10 and 11]. In addition, dump or sudden expansion combustors have been studied for integral rocket/liquid ramjet designs [Ref. 19].

The recirculation zone behind the bluff body or step causes intense mixing of fresh unburned fuel and air with hot combustion products. The hot combustion products ignite the fuel-air mixture. This stabilized flame can then propagate throughout the combustor. Due to the intense turbulent mixing in the recirculation zone, combustion may in some cases approach that of a well-stirred reactor.

A well-stirred reactor model considers the composition and all of the thermodynamic properties to be uniform throughout the volume. An idealized reactor with instantaneous mixing would have homogeneous fuel, air, and product concentrations, and constant pressure and temperature [Refs. 12 and 13].



Solid fuel ramjet combustors have, depending upon the combustor length and inlet configuration, two separate and distinct combustion zones, each of which appears to be controlled by a different mechanism [Ref. 9] (See Figure 1). In the recirculation zone products and reactants are rapidly mixed, and in the limiting case a well-stirred reactor may be approached. Downstream of the flow reattachment point the boundary layer develops and the combustion may be similar to that in a hybrid rocket in which kinetic effects are dominant (low pressure, high mass flux, severe oxidizer dilution).

Thus, one possible model for solid fuel ramjet combustion would be to treat the recirculation region as a well-stirred reactor and the downstream region as a kinetically dominated hybrid. The larger the grain length-to-diameter ratio, the more dominant the downstream region becomes in determining the average regression rate, and the more one could expect the ramjet to behave as a kinetically controlled hybrid combustor. However, for small L/D ratios and/or large recirculation zones, the combustion in the recirculation region may become important in determination of the average regression rate. In addition, the combustion characteristics in the recirculation region determine the flammability limits for the entire combustor. Thus, the model used in this region requires considerable attention. For very strong recirculation zones, a well-stirred reactor model may be adequate. However, for weaker recirculation



zones, which are desirable from a pressure loss standpoint, kinetic rates may be of the same order or greater than the reactant mixing rates. In this case, a well-stirred reactor model cannot be expected to be applicable and a more detailed consideration of the recirculating flow is necessary. Thus, the work of Gosman, et al. [Ref. 14] and Spalding, et al. [Ref. 15] becomes increasingly important and may provide the basis for modeling the recirculation region in solid fuel ramjet combustors.

It is the purpose of this study to determine the dependence of the regression rate of a solid fuel ramjet on chamber pressure, inlet air temperature, and mass flux of air, and to model the flow in the recirculation region caused by the sudden expansion inlet.



## II. METHOD OF INVESTIGATION

Non-burning flow visualization tests were conducted using a plexiglass model with three inlet step configurations. Flow reattachment points of the incoming stream were measured for various step Reynolds number flows.

A Fortran language computer program, Pistep II, developed by Spalding, et al. [Refs. 14 and 15] provided a finite difference solution of the two dimensional Navier-Stokes equations governing heat and mass transfer in recirculating flows. It was used to calculate the flow reattachment point and the flow field for non-burning flows. The results were compared with the flow visualization data and the work of previous investigators. The boundary conditions on the differential equations were altered to simulate blowing at the wall in order to study the effect of mass injection from the wall on the flow field.

Experimental firings were conducted using polymethyl-methacrylate grains burning with non-vitiated air to provide regression rate data as a function of inlet air temperature, chamber pressure, and oxidizer flux rate. These tests were made to provide initial data for characterizing ramjet combustion and flame blow-off limits, and to determine if the reacting flow behavior was similar to that obtained analytically and experimentally for non-burning flow.



### III. DESCRIPTION OF APPARATUS

#### A. COLD FLOW VISUALIZATION MODEL

The flow visualization model (Figure 2) consisted of three sections. The first section was a  $2\frac{1}{2} \times 2\frac{1}{2} \times 5$ -inch plexiglass block with a three-quarter inch diameter hole bored through the center. It received air from high pressure tanks and supported a perforated disk flow straightener. The step section was made of stainless steel and was ten inches in length to further dampen turbulence and provide fully developed velocity profiles. Three steps were used with inside diameters of 0.246, 0.519, and 0.714 inches respectfully. The third section was a  $15\frac{1}{2}$ -inch plexiglass tube with an inside diameter of 1.469 inches.

For the lower flow rates a sonic choke with a diameter of 0.081 inches was used to measure flow rates. For higher flow rates, an orifice flow meter with inputs to a Visicorder was used to measure flow rates. The flow reattachment points were measured visually using a scale.

#### B. HOT FIRING APPARATUS

A schematic of the solid fuel ramjet apparatus showing the overall system is presented in Figure 3.

##### 1. Ramjet Motor

The solid fuel ramjet motor consisted of four main sections: the head end assembly, the step insert section, the grain, and the aft closure section (Figure 4). All of

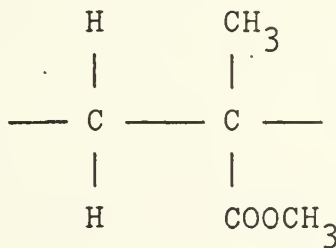


the metal parts of the motor except for the bolts were made of stainless steel.

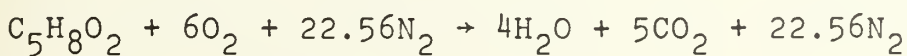
The head end assembly was 6 $\frac{1}{4}$  inches long and contained the inlets for the air, the oxygen-methane ignition mixture, the nitrogen purge, and the cooling air. Two Champion Z7 spark plugs were used for ignition.

The step insert section was 2-3/4 inches long and held the step in place. Three steps were used during this investigation with inside diameters of 0.25, 0.50, and 0.75 inches. This section also accommodated the forward end of the PMM grain.

Polymethylmethacrylate was chosen as the fuel in this study because it has been widely used for basic research in hybrid rocket combustion and in studies of polymer degradation in the past. It is composed of long chains of a repeating monomer:



Idealized chemical reaction with complete combustion would involve a stoichiometric reaction with air as follows:



The average molecular weight of the products in this case



is 31.3 lbm/lbmole. The gas constant is  $\bar{R}/M = 49.4$  ft-lbf/lbm-°R, and the stoichiometric air fuel ratio is 8.27 lbmair/lbmfuel. The equilibrium ratio of specific heats at a temperature of 3500°R is  $\gamma = 1.24$ . An adiabatic flame temperature calculation for the stoichiometric reaction using a value of  $\bar{H}_f^0$  of 92.8 kcal/mole for the heat of formation of PMM at 25 °C [Ref. 5] gives a flame temperature (with no dissociation) of 4265 °R.

The polymethylmethacrylate grains were cut from a slab into 3-3/4 x 3-3/4 x 12 inch blocks. The ends were rounded to an outside diameter of 3-1/2 inches to fit into the step section and the aft closure section, and were sealed with "O" ring seals. The initial inside port diameter of the grains was 1.5 inches. Eight grains were made that were six inches in length, but the majority of the tests were performed using grains that were 12 inches in length.

The aft closure section contained a straight section with a pressure tap and a converging-diverging nozzle. Nine nozzles with various throat areas were used to control the chamber pressure. A Wiancko 0-200 psig pressure transducer was mounted on the forward part of the aft closure section to measure the chamber pressure.

The grains were held in place by four 3/8 inch diameter steel rods between the step section and the aft closure section. Mounting flanges on the head end assembly and the aft closure section were bolted to a large test stand.



## 2. Ignition System

The ignition system metered oxygen and methane at 800 psig from two high pressure tanks through needle valves into the head end assembly section. Inlet ports on the top and the bottom injected methane, and two inlet ports injected oxygen from either side. Two inches downstream from the oxygen-methane ports were two Champion Z7 spark plugs located 180 degrees apart. A transformer supplied power to a Model T spark coil to energize the spark plugs.

## 3. Nitrogen Purge and Cooling Air System

The nitrogen purge and cooling air system was connected upstream of the head assembly section. Two high pressure tanks fed nitrogen into the motor at the end of a hot firing for approximately one second to extinguish the combustion flame. Cooling air from a low pressure compressor was then blown through the motor.

## 4. Air Flow Control

A standard ASME orifice flow meter was used to measure the flow rate of the air into the motor. A manually operated gate valve between the orifice and the motor was used to provide the desired flow rate through the motor. Two pneumatically operated Jamesbury ball valves operating together either vented the air to the atmosphere, or allowed the air to pass through the motor.

## 5. Data Acquisition System

A Colvin 0-35 psi differential pressure transducer was used to measure the pressure drop across the orifice



flow meter. A Wiancko 0-200 psig pressure transducer was used to measure the pressure upstream of the orifice, and an iron-constantan thermocouple was used to measure the temperature at the orifice. A second iron-constantan thermocouple was used to measure the temperature of the air entering the motor. A Wiancko 0-200 psig pressure transducer measured chamber pressure at the aft closure section of the motor.

The orifice thermocouple output was recorded on a 0-600°F strip chart recorder. All of the other transducer outputs were recorded on a Honeywell Model 2106 Visicorder. A five cycle per second timing signal and an ignition pulse were also recorded on the Visicorder.

## 6. Air Feed System

A Pennsylvania air compressor provided air at pressures up to 150 psia at a rate of up to 700 scfm. This air was fed into an air reservoir and a Polytherm air heater. The Polytherm air heater was capable of yielding 1.75 pounds per second airflow at 150 psia and 1000°F. The heater burned natural gas, and the air passed through a heat exchanger, thus providing non-vitiated hot air.

A temperature controller directed two mixing valves that produced the required air temperature at 150 psia. A manual gate valve controlled the air flow to the test cell. A valve in the test cell controlled the flow of air to the pipe leading to the orifice flow meter.

Figures 5, 6, 7, and 8 show the test cell and the ramjet apparatus.



#### IV. EXPERIMENTAL PROCEDURE

##### A. COLD FLOW TESTS

The cold flow tests were performed at the rocket lab facilities of the Naval Postgraduate School. Visualization was obtained by injecting a mixture of water, alcohol, and food coloring at the base of the step inlet through a small tube with a hypodermic needle. The mixture was broken up into very small droplets by the turbulence in the recirculation zone. In the recirculation zone the droplets on the wall moved towards the step. At the flow reattachment point the droplets on the wall were stationary. Downstream of the reattachment point the droplets on the wall moved away from the step. Using this technique, the flow reattachment point locations for various step Reynolds number flows using three step sizes were measured visually using a scale.

Initial visualization tests were attempted using a tufted model but they proved to be of limited value due to the highly turbulent nature of the flow.

##### B. HOT FIRING TESTS

All hot firing tests were performed in the jet engine test cell at the Naval Postgraduate School. Hot firing data were obtained from a series of firings at three air flow rates, three chamber pressures, and three inlet temperatures, using three step heights and two grain lengths. The majority of the hot firings were performed with a 12 inch



grain length and an inlet diameter of 0.5 inches. Table I summarizes the nominal test conditions.

TABLE I  
NOMINAL TEST CONDITIONS

---

Chamber Pressure (psia)	50	75	100
Air Flow Rate (lbm/sec)	.15	.25	.40
Inlet Temperature (°F)	70	200	350
Inlet Diameter (in)	.25	.50	.75
Step h/D	.417	.333	.25
Grain Length (in)	12	6	

---

For the tests in which the Polytherm air heater was used, the temperature controller was set and the temperature would stabilize at the ramjet inlet in one to two hours. This delay was due to the fact that the flow rates to the motor were quite low, at most 0.5 lbm/sec. Once the temperature stabilized at the desired temperature at the inlet to the ramjet, the manual gate valve downstream of the orifice was set to obtain the desired air flow rate.

Chamber pressures were preselected and controlled by varying the nozzle throat area for a given air flow rate. Chamber pressures could normally be attained within ten psi of the desired pressure. Calculated combustion temperatures



varied significantly with air flow rate and step size. Also, at higher chamber pressures the preset flow rate would decrease upon ignition because the higher back pressure would unchoke the air flow control valve.

Ignition normally lasted for four seconds. After three seconds of ignition, the air was directed through the ramjet motor. Ignition was continued into the first second of the run to insure that combustion would be sustained. A series of thirteen tests at high flow rates in which the ignition flame was blown out were used to determine the rate of consumption of the PMM grains during the oxygen-methane ignition. These data were used to correct the initial weight of the fuel used in the regression rate calculation.

Combustion lasted for thirty seconds. At the end of each run the motor was extinguished by simultaneously venting the air to the atmosphere with the Jamesbury ball valves and actuating the nitrogen purge system. Low pressure air was then blown through the motor for cooling. The only section of the motor that heated up significantly was the aft closure section and the nozzle.



## V. PISTEP II COMPUTER PROGRAM

Pistep II is a Fortran computer program developed by Gosman, Pun, Runchal, Spalding, and Wolfshtein [Ref. 14]. It provides a finite difference solution of a steady incompressible turbulent flow through a cylindrical pipe with a sudden step enlargement. Equations [Ref. 15] governing the distribution of stream function,  $\psi$ , vorticity,  $\omega/r$ , non-dimensional temperature,  $T$ , turbulent kinetic energy,  $k$ , and turbulent energy dissipation rate,  $\epsilon$ , are cast in elliptic form in cylindrical polar coordinates as follows:

$$a_\phi \left[ \frac{\partial}{\partial z} \left( \phi \frac{\partial \psi}{\partial r} \right) - \frac{\partial}{\partial r} \left( \phi \frac{\partial \psi}{\partial z} \right) \right] - \frac{\partial}{\partial z} \left[ b_\phi r \frac{\partial (C_\phi \phi)}{\partial z} \right] - \frac{\partial}{\partial r} \left[ b_\phi r \frac{\partial (C_\phi \phi)}{\partial r} \right] + r S_\phi = 0$$

where  $\phi$  represents any one of the variables  $\psi$ ,  $\omega/r$ ,  $k$ ,  $\epsilon$ , or  $T$ . The functions  $a_\phi$ ,  $b_\phi$ ,  $C_\phi$ , and  $S_\phi$  are presented in Table II.

A two equation turbulence model is employed in the program. The two variables are turbulent kinetic energy,  $k$ , and the turbulent energy dissipation rate,  $\epsilon$ . The effective viscosity,  $\mu_{eff}$ , is related to  $k$  and  $\epsilon$  by

$$\mu_{eff} = C_\mu \rho k^2 / \epsilon$$



A "dissipation length scale",  $\ell$ , can be used in an alternative formulation:

$$\mu_{\text{eff}} = C_{\mu} k^{1/2} \rho \ell$$

Equating the two equations for the effective viscosity gives:

$$\ell = k^{3/2} / \epsilon$$

Constants that appear in the two turbulence equations are  $c_1$ ,  $c_2$ ,  $c_{\mu}$ ,  $\sigma_k$ , and  $\sigma_{\epsilon}$ . Values used in the computer program together with their Fortran symbols are given in Table III.

TABLE II  
VARIABLE FUNCTIONS (Table I of Ref. 15)

$\phi$	$a_{\phi}$	$b_{\phi}$	$c_{\phi}$	$s_{\phi}$
$\omega/r$	$r^2$	$r^2$	$\mu_{\text{eff}}$	0
$\psi$	0	$1/\rho r^2$	1	$-\omega/r$
$k$	1	$\mu_{\text{eff}}/\sigma_k$	1	$-(G - \rho \epsilon)$
$\epsilon$	1	$\mu_{\text{eff}}/\sigma_{\epsilon}$	1	$-(c_1 G \epsilon / k - c_2 \rho \epsilon^2 / k)$
$T$	1	$\mu_{\text{eff}}/\sigma_h$	1	0

$G$  is a generation term:

$$G = \mu_{\text{eff}} \{ 2 \left[ \left( \frac{\partial V_z}{\partial z} \right)^2 + \left( \frac{\partial V_r}{\partial r} \right)^2 + \left( \frac{V_z}{r} \right)^2 \right] + \left[ \frac{\partial V_z}{\partial r} + \frac{\partial V_r}{\partial z} \right]^2 \}$$



TABLE III  
TURBULENCE CONSTANTS (Table II of Ref. 15)

Constant	$c_1$	$c_2$	$c_\mu$	$\sigma_k$	$\sigma_\epsilon$
Fortran Symbol	C1	C2	CMU	PR(NK)	PR(NE)
Value	1.45	2.0	0.09	1.0	1.3

Boundary conditions are specified at every point on the boundary. Wall functions that are derived from Couette flow solutions are used in evaluating boundary values for  $w/r$ ,  $k$ ,  $\epsilon$ , and  $T$ . Other boundary conditions are given in Figure 9.

The computer program calculates heat and momentum transfer in steady two-dimensional axisymmetric recirculating flows. Five simultaneous coupled non-linear partial differential equations are solved. The finite difference equations are implicit equations that are coupled and non-linear. The Gauss-Seidel point iterative method is used to solve the finite difference equations. Provisions are made for both overrelaxation and underrelaxation of the variables.

References 14 and 15 contain a more complete discussion of the mathematical formulation of the problem, development of the finite difference equations, and solution algorithms. An excellent discussion of several turbulence models can be found in Reference 16.



The boundary conditions on the pipe wall can be changed so that the effect of mass addition through the wall for non-reacting flows can be investigated analytically. A constant radial velocity at the wall, which yields a linearly varying stream function along the wall, is used to simulate wall mass injection (See Figure 10). In this initial study, the main flow and the wall mass addition were identical in chemical composition and temperature.

In Pistep II, wall functions based on Couette flow are used to specify the boundary conditions on the pipe wall for all of the variables except stream function. For very low blowing rates, which are characteristic of solid fuel ramjets, Couette flow solutions may yield realistic results. However, for higher mass injection rates, Couette flow solutions may not adequately represent the boundary conditions.

The centimeter-gram-second system of units is used in the Pistep II computer program.



## VI. RESULTS AND DISCUSSION

### A. COLD FLOW EXPERIMENTS

A series of cold flow visualization tests were conducted to determine the reattachment point location for flow over a rearward facing step at the inlet of a cylindrical tube.

Defining a step Reynolds number as:

$$Re_{step} = \frac{\rho V h}{\mu} \quad \text{where}$$

$\rho$ ... fluid density

$V$ ... average velocity in the port of the tube

$h$ ... step height

$\mu$ ... fluid viscosity

it was found that the reattachment point location remained constant as the step Reynolds number was changed for a given step height. The reattachment point moved further downstream with increasing step height. The tube inside diameter was used to non-dimensionalize the reattachment point location from the face of the step. A linear least-square curve fit of 47 data points was used to obtain the following equation (See Figure 11).

$$\frac{x_r}{D} = 7.15 (h/D) + 0.35$$

Figure 12 compares the data obtained in this investigation with the data of Abbott and Kline [Ref. 1] and Krall and



Sparrow [Ref. 2]. The unsymmetric reattachment points obtained by Abbott and Kline are shown. The flow reattached at different locations on either side of the two-dimensional channel. The location of the maximum heat transfer coefficient found by Krall and Sparrow for water flow through an orifice in a cylindrical tube was used to locate the reattachment point data shown in Figure 12.

The data from this study fell between that of Krall and Sparrow and the downstream reattachment point found by Abbott and Kline. Air was used in this study whereas water was used in the other studies; however, each study found that reattachment point location was not affected by changing Reynolds number for a constant step height. Krall and Sparrow also found that changing Prandtl number of the flow did not change the reattachment point location.

The spread in the cold flow data in Fig. 11 is probably due to larger relative errors in measurement closer to the step face and not due to Reynolds number effects.

At higher step Reynolds numbers small vortices were observed at the step face similar to the observations of Abbott and Kline for two-dimensional channel flow. The reattachment point was axially symmetric for most Reynolds number flows. However, at high Reynolds numbers the reattachment point varied around the circumference of the tube. Four distinct lobes could be seen when this occurred and may be associated with the small vortices at the step face. It



was also observed that the rotation and mixing of the flow in the recirculation zone became more intense as the height of the step increased.

## B. PISTEP II RESULTS

The Pistep II computer program was run for four step configurations and five inlet velocities. Table IV summarizes the reattachment point results. A linear least-square curve fit is shown in Figure 11 and Figure 12 for comparison with the cold flow data and the data from other investigations. From these figures it is seen that Pistep II gives a dependence of  $X_r/D$  on  $h/D$  which is in general agreement with experimental results. With the current turbulence model and wall functions, the results agree closely with those of Krall and Sparrow and fall somewhat below the data obtained in this investigation.

A 21 x 21 grid was used for the  $h/D$  of .25 and a grid of 20 x 20 was used for the other values of  $h/D$ . The computing time required for each run was on the order of 20 to 30 minutes. Underrelaxation of the variables was required to ensure numerical stability. Even with underrelaxation, the case with  $h/D$  of 0.421 was numerically unstable for most of the inlet velocities tried. However, this case converged the fastest when numerically stable.

At each of the grid points, Pistep II calculated the distribution of the following parameters: vorticity, stream function, turbulent kinetic energy, turbulence dissipation



TABLE IV  
RESULTS OF PISTEP II CALCULATIONS

$h/D$	$X_r/D$	$Re_{step}^*$	Niter**	$V_{in}$ (cm/sec)
.250	1.735	2446	900	1524
.250	1.696	12232	700	7620
.250	1.761	24465	900	15240
.250	1.702	36698	700	22860
.289	1.979	2009	800	1524
.289	2.008	20089	800	15240
.289	2.004	31033	800	22860
.342	2.152	1335	700	1524
.342	2.199	6677	800	7620
.342	2.161	13354	700	15240
.342	2.215	20032	800	22860
.421	2.705	4109	523	15240
.421	2.708	6163	521	22860

\* Based upon a fixed laminar viscosity of  $1.78 \times 10^{-4}$   
gm/cm.sec

\*\* Niter is the number of iterations



rate, non-dimensional temperature, axial velocity, radial velocity, effective viscosity, density, and turbulence length scale. Variations of shear stress and heat transfer coefficient along the walls were also calculated. The location of the flow reattachment point was determined by solving for the point at which the wall shear stress was zero.

#### C. PISTEP II WITH WALL MASS ADDITION

The boundary conditions were altered along the "north" wall as shown in Figure 10. A linearly varying stream function (i.e., a constant radial velocity at the wall) was used to simulate injection of mass uniformly through the wall. For this initial study, the chemical composition of the mass injected through the wall was chosen to be identical to that of the main stream coming in the inlet. FAR is a term that is analogous to a fuel air ratio, and represents the fraction of the total incoming inlet stream that is injected through the wall. For example, FAR = 0 gives no wall mass injection. FAR = 0.5 gives an amount of wall mass injection equal to half of the inlet stream so that the amount leaving at the exit is 1.5 times the amount entering at the inlet.

FAR was varied in increments of 0.1 for the case in which inlet velocity was 500 ft/sec ( $V_{IN} = 15240$  cm/sec) for an  $h/D$  of 0.342. Stream function output was punched onto cards which were used as input for a separate program



which generated contours of streamlines using the Calcomp plotter (see Appendix A). Figures 13 through 21 show the streamline patterns obtained for various conditions. It should be noted that the streamline patterns are shown only for the upstream half of the ramjet and that the radial coordinate has been expanded more than the axial coordinate so that the figures are not to scale. This permits a better visual presentation of the streamlines in the recirculation zone. Note that with wall mass addition (Figures 14 through 18), a streamline that originates on the north wall in the recirculation region escapes from the recirculation zone and enters the main stream of flow. Figures 20, 13, and 19 show the effect of increasing step size ( $h/D$ ) while maintaining inlet velocity constant (mass flow rate decreases). Comparison of Figures 20 and 21 shows the effect of decreasing inlet velocity (or inlet mass flow) with a fixed  $h/D$  and comparison of Figures 13 and 21 shows the effect of decreasing step size with a fixed inlet mass flow rate.

Table V summarizes the results for wall mass addition. The reattachment point location, based on the point where wall shear stress is zero, moves upstream slightly as wall blowing is increased. The "wall shear stress" is calculated from the stream function difference between the wall node and the first node out from the wall. In the tube between these two nodes the axial velocity is at least an order of magnitude greater than the radial velocity. This permitted the calculation of the "reattachment point" in the same



manner as for no blowing. Also, the magnitude of the radial velocity at the wall is quite small compared to the magnitude of the inlet velocity. It should be emphasized that these results were obtained using the same boundary conditions on  $\omega/r$ ,  $T$ ,  $\epsilon$ , and  $k$  as for no blowing. Further studies are required to determine whether or not this assumption is realistic.

TABLE V

PISTEP II WITH WALL MASS ADDITION ( $h/D = 0.342$ )

$V_{in}$ (cm/sec)	FAR	$x_r/D$	$V_{wall}$ (cm/sec)
15240	0.0	2.211	0.0
15240	0.1	2.191	4.7
15240	0.2	2.168	9.5
15240	0.3	2.145	14.2
15240	0.4	2.123	19.0
15240	0.5	2.101	23.7

Note: 900 iterations for each of the above runs

#### D. PMM/AIR RAMJET

Seventy-four hot firing tests were conducted. A Fortran language computer program was written to reduce the data. A computer listing together with the output is included in



Appendix B. The first three pages of the output tabulate the measured data for each test in which combustion was sustained. This is followed by the calculated results. This program was modified to reduce the data for the tests in which combustion was not sustained. A computer listing and output for the non-sustaining tests is included in Appendix C.

The expected uncertainties in the experimental results was calculated using the error analysis method of Kline and McClintock [Ref. 17]. Using the notation defined in the ramjet data reduction computer program, the uncertainties are given in Table VI.

The step inlet caused non-uniform regression of the fuel grains. There was less regression of the fuel at the head end in the recirculation region, and nearly uniform regression downstream of the reattachment point, where regression rate was observed to decrease slightly with increasing distance from the head end. The inlet effect was more pronounced for larger values of  $h/D$ . For the majority of the tests there was a significant amount of carbon deposited on the surface of the fuel at the head end. The reattachment point locations were measured to the edge of the carbon deposits or to the location of maximum regression. These two locations were nearly coincident in most cases. The regression patterns for three tests are shown in Figure 22.

Regression rates were calculated using two methods. Based upon the exit diamter, average regression rate can



TABLE VI  
ERROR ANALYSIS

Symbol	% Error	Variable
WDOT	6.3	air weight flow rate
TC	13.8*	calculated chamber temperature
RDE	1.4	$\dot{r}$ based on exit diameter
RWT	1.1	$\dot{r}$ based on weight loss
WF	.6	fuel weight flow rate
FG	8.6*	gross thrust
FISP	8.6*	fuel specific impulse
RESTEP	5.8	step Reynolds number
GAIR	5.7	air flux rate
UPORT	15.0*	average port velocity
SFC	8.6*	specific fuel consumption
EQN	11.0	empirical $\dot{r}$ equation

\* The uncertainty in the ratio of specific heats,  $\gamma$ , and the gas constant,  $R$ , were not included in this analysis. Complete expansion through an ideal nozzle was assumed in calculating FG, FISP, and SFC.



be defined by:

$$\dot{r} = \frac{d_f - d_i}{2 \Delta t} \quad (\text{in/sec})$$

where  $d_i$  and  $d_f$  are the initial and final exit diameters before and after firing, and  $\Delta t$  is the burn time. An average regression rate based on weight loss of the fuel can also be calculated:

$$\dot{r} = \sqrt{\frac{4 (W_i - W_f)}{\pi \rho L} + \frac{d_i^2 - d_i}{2 \Delta t}} \quad (\text{in/sec})$$

where  $W_i$  and  $W_f$  are the initial and final weights of the grain,  $\rho$  is the density of the fuel, and  $L$  is the grain length. This expression for the regression rate gives a better average value when there is non-uniform regression along the length of the grain, and was used throughout this investigation.

The dependence of the regression rate of the fuel on chamber pressure,  $P$  (psia), inlet air temperature,  $T$  ( $^{\circ}$ R), and average mass flux of air,  $G$  (1bm/in $^2$ sec), was determined by holding two of these parameters at fixed values and varying the third for several tests. It was found that the regression rate varied as:

$$\dot{r} = C P^{0.51} T^{0.34} G^{0.41} \quad (\text{in/sec})$$



where C is a proportionality constant. For a step h/D of 0.333,  $C = 2.3 \times 10^{-4}$  and for a step h/D of 0.416,  $C = 3.4 \times 10^{-4}$ . A plot of the regression rate based on weight loss,  $\dot{r}_{wt}$ , versus this empirical regression rate equation is shown in Figure 23. On the sixth page of the ramjet data reduction computer program output in Appendix B, the numerical results are tabulated. The expected uncertainty in the empirical equation was calculated to be 11%.

Muzzy [Ref. 4] has shown that the regression rate equation for a hybrid rocket operating in the kinetically dominated region can be expressed as:

$$\dot{r} = C P^{0.5} G^a X^b$$

where a varies from 0.3 to 0.4 and b varies from -0.1 to -0.2, and X is the longitudinal coordinate.

Thus, the average regression rate of the fuel in a solid fuel ramjet is very similar to that for pressure sensitive hybrid rocket combustion. This is not surprising since the reattachment point normally occurred at less than one-fourth



of the grain length. Aft of the reattachment point combustion should approach that of a kinetically controlled hybrid combustor.

The maximum regression rate of the fuel occurred near the location of the flow reattachment point. This is due to several factors. More oxidizer reaches the wall from the impingement of the main oxidizer stream at the reattachment point. In addition, the maximum Nusselt number occurs near the reattachment point location.

Data from 36 of the tests in which combustion was not sustained are tabulated with the computer program in Appendix C. For the smallest step  $h/D$  used (0.25), combustion was sustained only while the ignition system was operating. As soon as ignition was terminated, the flame blew off. For the middle step ( $h/D = 0.333$ ) the flame blew off as soon as the air flow was activated for many of the tests at higher flow rates. Some of the tests in which combustion was not sustained may have been due to insufficient ignition prior to activating the air flow.

Tests performed at the United Technology Center [Ref. 8] have indicated that inlet configuration is more important in determining when combustion will be sustained. A critical step  $h/D$  ratio was found to be the best criterion. For values of  $h/D$  less than the critical value, combustion could not be sustained. It was reported that for one particular all-hydrocarbon fuel the critical  $h/D$  was 0.14. For polymethylmethacrylate they found that the critical  $h/D$



was 0.31. This criterion did not vary with step Reynolds number.

The data from this investigation indicated that for high inlet velocities with  $h/D$  greater than the critical value determined by UTC, combustion may not be sustained. It appears that not only is  $h/D$  important, but inlet velocity, ignition time, and inlet temperature may also be important. At identical air mass flow rates, some of the tests at higher inlet temperatures failed to sustain combustion. This is probably a velocity effect since at constant mass flow rates, increasing temperature increases the velocity.

The Pistep II results, although for non-burning cases, should indicate trends to be expected in the burning tests. The data indicate that the magnitude of the velocity at a point in the recirculation zone is directly proportional to the inlet velocity. Also the velocity in the recirculation zone  $V$ , was found to be inversely proportional to  $h/D$ . Thus  $V \propto V_{IN}$  and  $V \propto 1/(h/D)$ . It was also found that  $\frac{X_r}{D} \propto \frac{h}{D}$  but did not vary with inlet velocity.

A simplified model of the flame stabilization region is one in which the recirculation zone is considered as an ignition zone whose length,  $L$ , corresponds to the reattachment point location. At the flame blowoff condition, the gases traveling through the recirculation zone have an average contact time equivalent to the ignition time of the gases:  $t_c = t_i$ . If  $V$  is a characteristic velocity



in the recirculation zone, then  $t_c \propto L/V$ . Since

$$V \propto \frac{VIN}{h/D}$$

and

$$L \propto X_r/D \propto h/D$$

then one possible expression for contact time is

$$t_c \propto \frac{(\frac{h}{D})^2}{VIN}$$

The step  $h/D$  has a more dominant effect in determining flammability limits, however inlet velocity is also important. This treatment is oversimplified and was discussed only to indicate that the inlet velocity may be of significance in determining blowoff limits. In actuality, ignition time is a function of the fuel-air ratio in the recirculation zone and this is in turn a function of  $h/D$ . Thus, the functional form becomes more complex as one considers the details of the recirculation region.

It should also be noted that the simplified model described above neglects the effects of turbulence intensity on flame stabilization. Examination of Pistep II output indicates that for a constant inlet mass flow rate, increasing step height increases both the turbulent kinetic energy and



the turbulence dissipation rate. Also for a fixed inlet velocity, increasing step height decreases the recirculation zone velocity, the turbulent kinetic energy and the turbulence dissipation rate.

There are three blow-off situations to be considered. The first one is a steady-state blowoff limit that occurs when the mass flow rate in the recirculation zone is greater than the mass consumption rate by chemical reaction. The mass flow rate through the zone will depend upon the size of the zone and the velocity through the zone. This may be important in throttling applications during normal combustion. The second situation is one in which there are ignition transient blowoff limits during starting. Low chamber pressure during ignition gives higher inlet velocities which may cause the flame to blowoff even though combustion would sustain if ignition occurred at the expected operating pressure. Thirdly, it is possible that the flow at the step inlet may become choked at high mass flow rates when the chamber pressure is low during ignition. Subsequent expansion could modify the size and flow characteristics of the recirculation zone and cause the flame to blowoff. This indicates that if a ramjet operating with high flow rates could be started at a higher chamber pressure, combustion may be sustained.

The Pistep II computer program should prove to be advantageous in studying blowoff limits. When chemical reaction and wall mass injection are included in the



program, blowoff velocities in the recirculation zone could be realistically studied. The effect of  $h/D$ , inlet velocity (or mass flow rate), and chemical reaction rate could be considered. Blowoff limits have been calculated in this manner for premixed gases in a dump combustor [Ref. 15].

If the results of Abbott and Kline [Ref. 1] are similar to what may be expected in an axisymmetric situation with combustion, inlet turbulence would not be expected to affect the recirculation zone. However, inlet turbulence may affect the regression rate of the fuel downstream of the reattachment point. Further tests are needed to clarify the affects of inlet turbulence and distortion on solid fuel ramjet combustion.



## VII. CONCLUSIONS

The cold flow visualization data were in general agreement with previous studies. Reynolds number had no measurable effect on the size of the recirculation zone and the reattachment point location. The reattachment point moved further downstream from the face of the step as step height increased.

The Pistep II computer program appears to predict with acceptable accuracy the reattachment point locations for non-reacting flows with no wall mass addition. Pistep II, modified for wall mass addition, indicated that the size of the recirculation zone and the reattachment point location are not greatly affected by wall mass addition. The location of the reattachment point moved slightly closer to the step face as wall blowing was increased. Experiments are required to verify this result, and the assumptions concerned with the boundary conditions used in the computer program require further investigation. The Pistep II computer program has proven to be accurate enough to warrant further development as a ballistics program for the recirculation region.

Solid fuel ramjets which use PMM as the fuel have an average regression rate that follows the expression:  
$$\dot{r} = C P^{0.51} T^{0.34} G^{0.41}$$
. In addition, the maximum regression occurred near the reattachment point location. Downstream of the reattachment point the regression rate



decreased slightly with increasing distance from the head end. Thus, solid fuel ramjets have an average regression rate that closely follows the theoretical expression derived for kinetically controlled hybrid rocket combustion.

The step  $h/D$  is the dominant parameter in determining flame stability limits; however, inlet velocity is also an important parameter.

The results of this investigation indicate that a reasonable internal ballistics model for solid fuel ramjets may be obtained by using the Pistep II computer program (modified for chemical reactions and wall mass addition) together with the regression rate equation for kinetically controlled hybrid rocket combustion. The modified Pistep II program should be used to analyze the recirculation region (blowoff limits, etc.) and to provide the input data (chemical composition, etc.) to the regression rate equation for kinetically controlled hybrid rocket combustion. The latter should be employed downstream of the reattachment point.



## VIII. SUGGESTIONS FOR FUTURE WORK

This work was an initial study of the internal ballistics of solid fuel ramjets. Additional experimental and analytical studies are required in order to a) obtain increased combustion efficiency, b) refine the internal ballistics model and c) study the effect of other inlet geometries and flow conditions on the regression rate of the fuel. Specific experimental studies needed include determination of a) the effect of wall mass addition on the recirculation zone for a step inlet using inert flows (to compare with the theoretical predictions using Pistep II), b) the effect of different inlet configurations such as swirl vanes and plug inlets on fuel regression rate and flame stability limits, and c) the effect of different mixing techniques on combustion efficiency. Analytical studies required are a) modifications to the Pistep II computer program to include chemical reaction with heat and mass transfer at the wall and b) combination of the recirculation zone model (as input) with the kinetically controlled hybrid combustion model to effect a usable internal ballistics model for solid fuel ramjets.



HIGHLY TURBULENT RECIRCULATION  
ZONE (MAY APPROACH A  
WELL-STIRRED REACTOR)

DIFFUSION FLAME LOCATED IN  
TURBULENT BOUNDARY LAYER WITH  
HIGH DEGREE OF OXIDIZER DILUTION

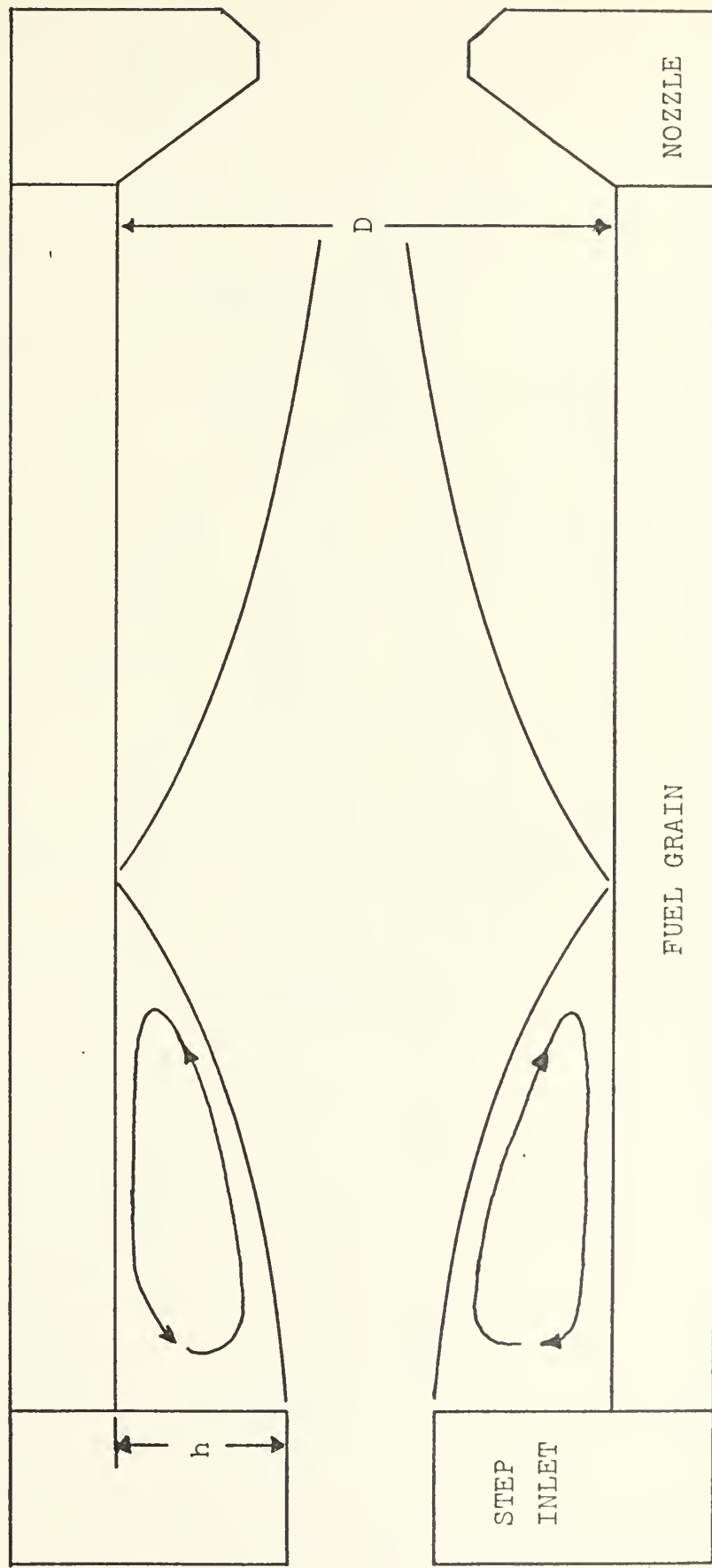


FIGURE 1. COMBUSTION MECHANISMS



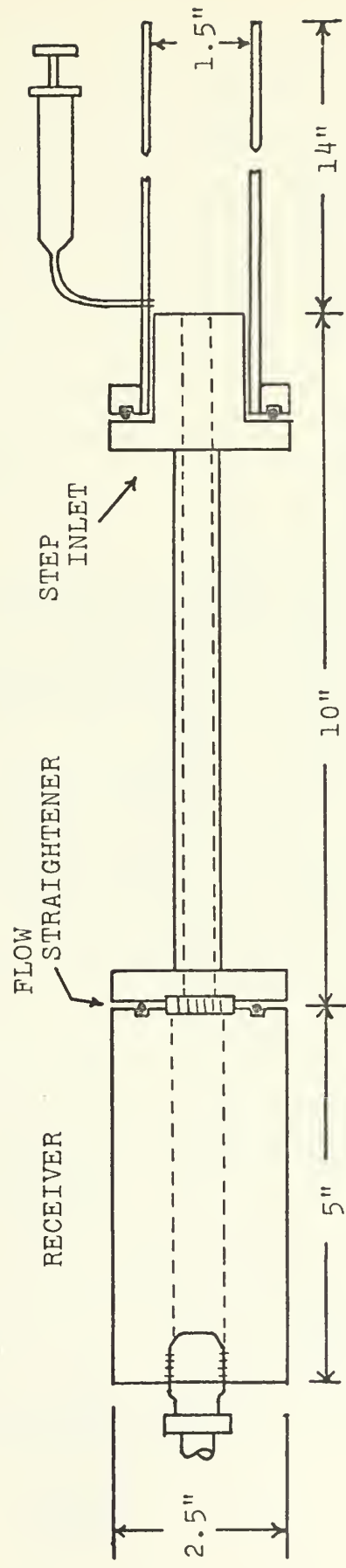


FIGURE 2. COLD FLOW VISUALIZATION APPARATUS



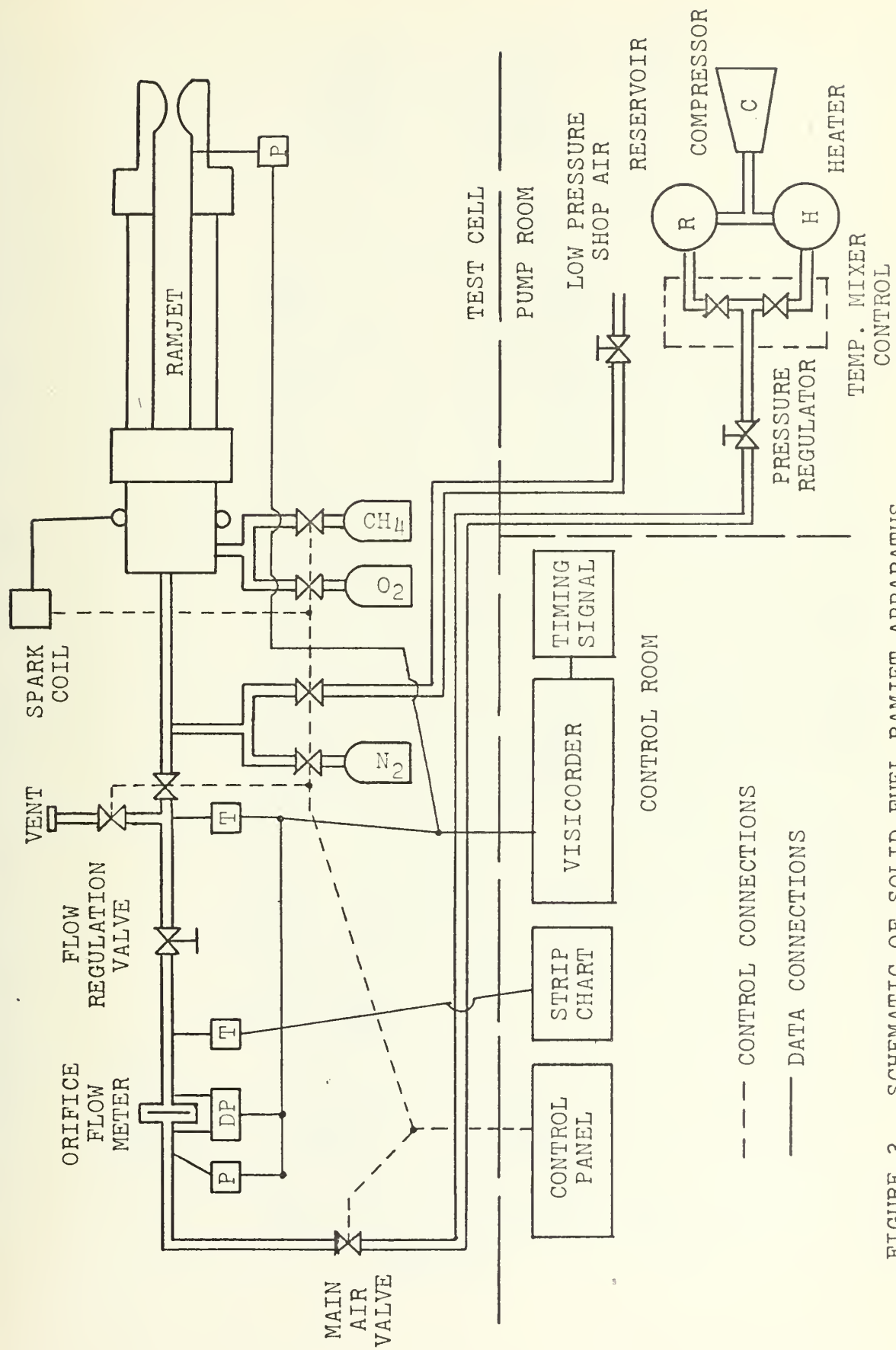


FIGURE 3. SCHEMATIC OF SOLID FUEL RAMJET APPARATUS



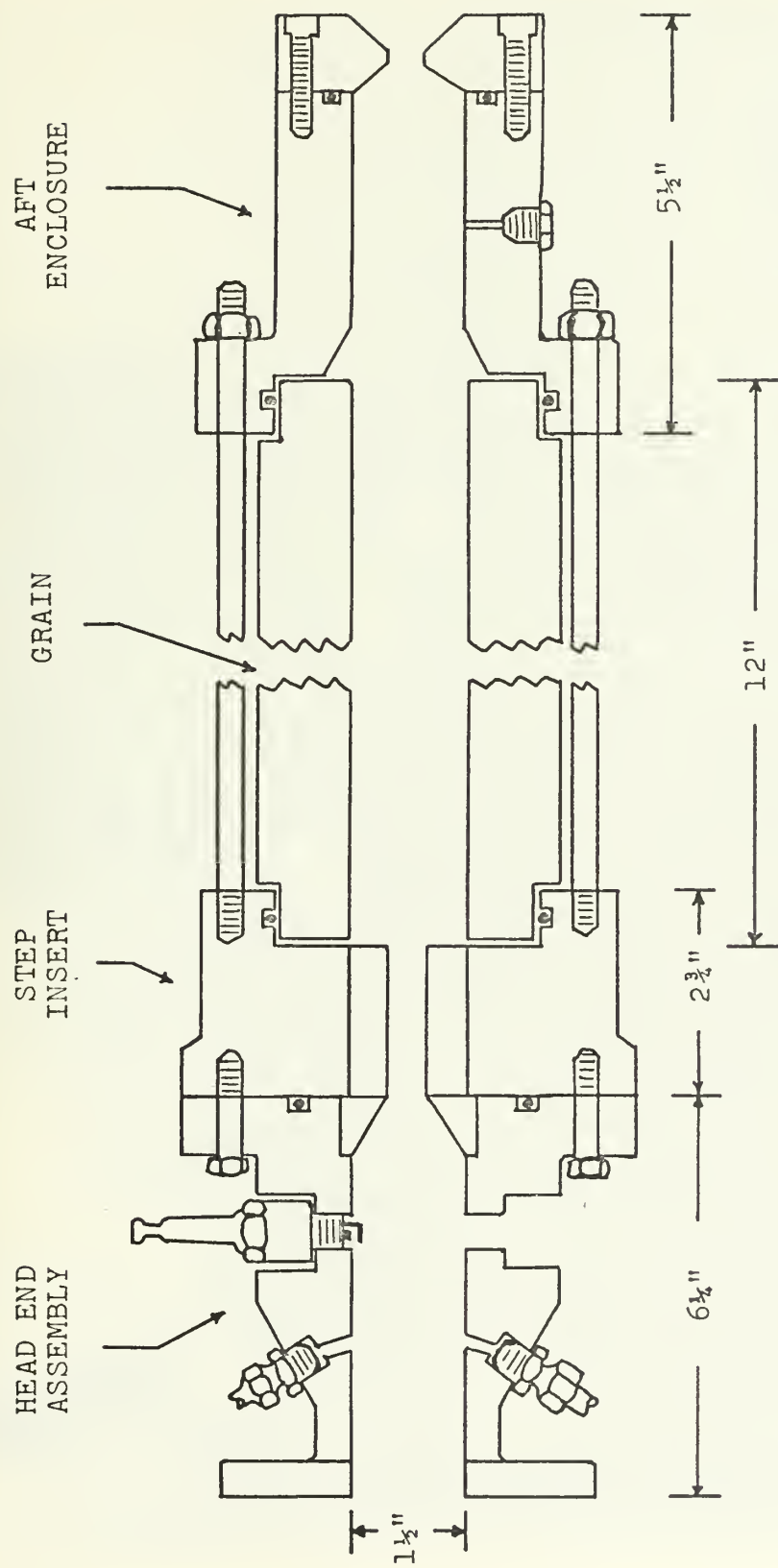


FIGURE 4. SOLID FUEL RAMJET MOTOR



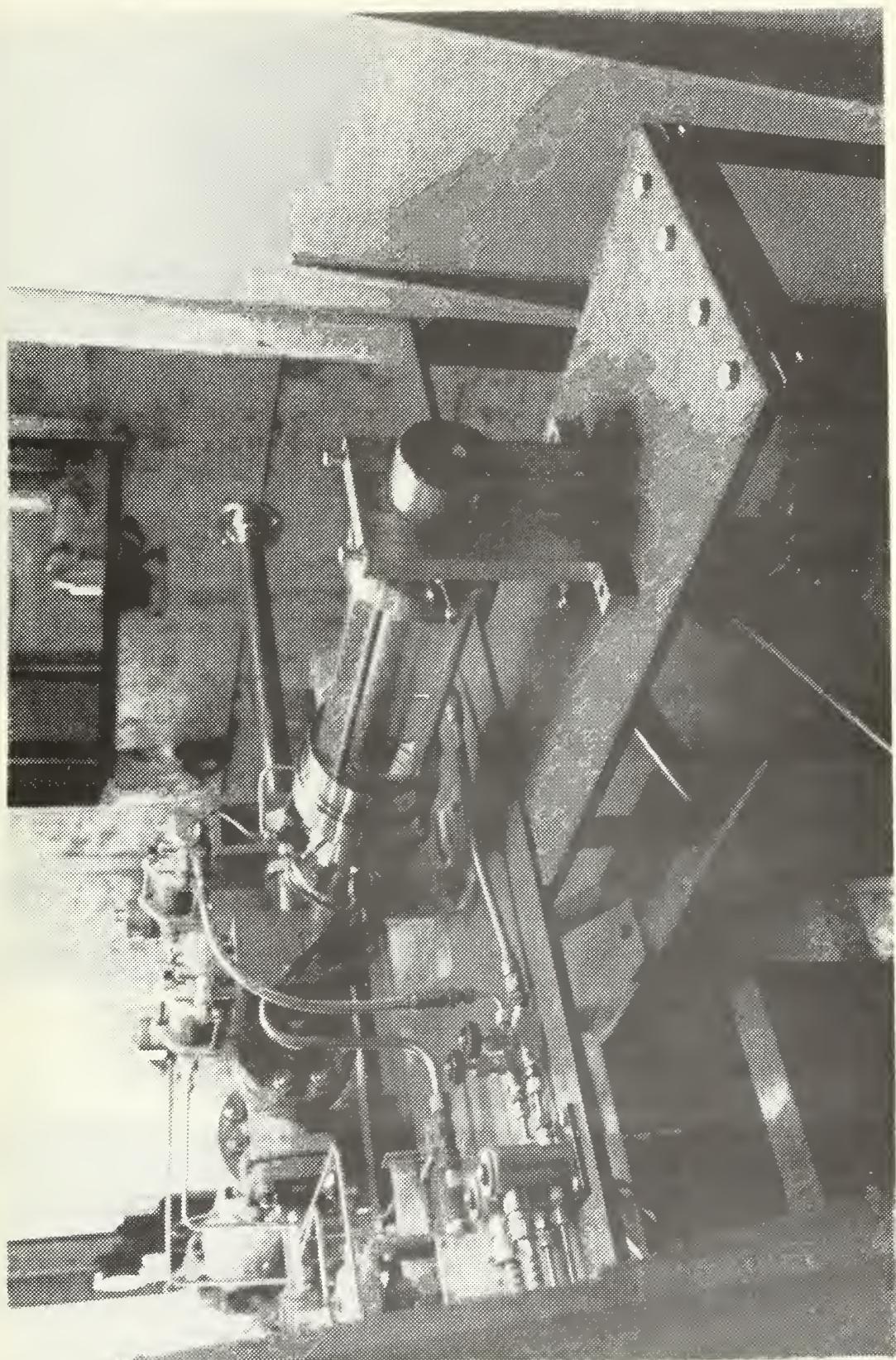


FIGURE 5. RAMJET MOTOR ON TEST STAND



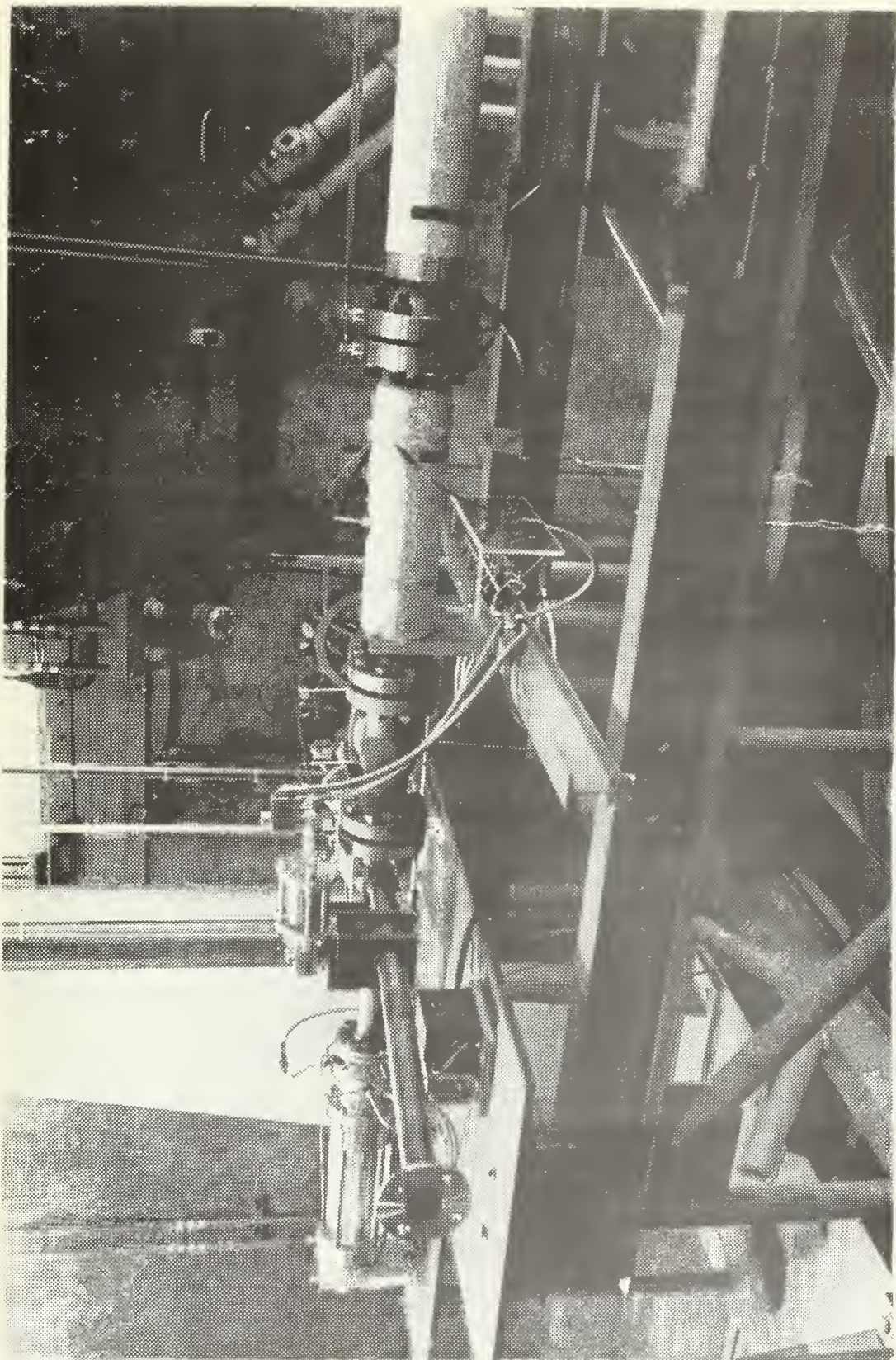


FIGURE 6. TEST STAND



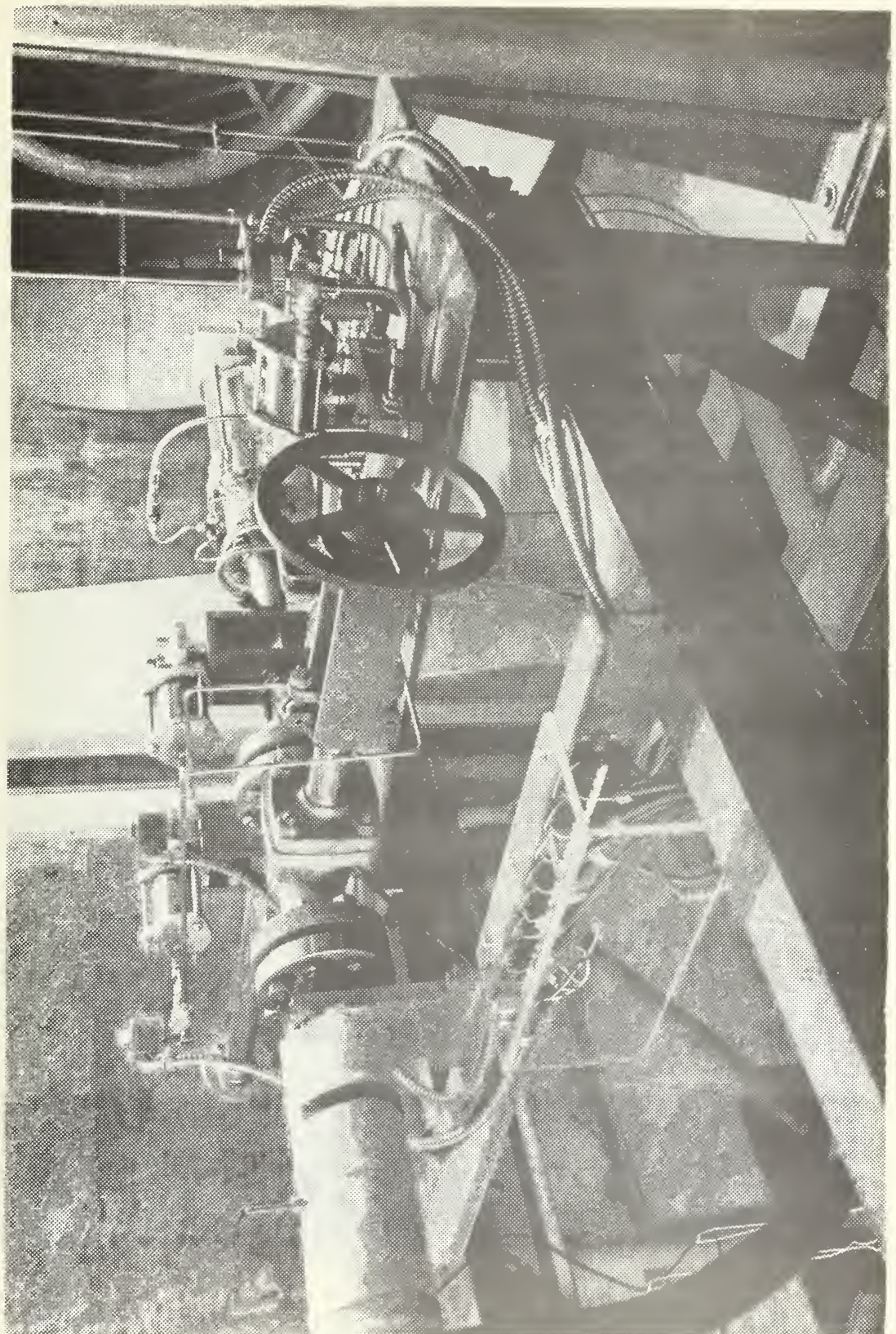
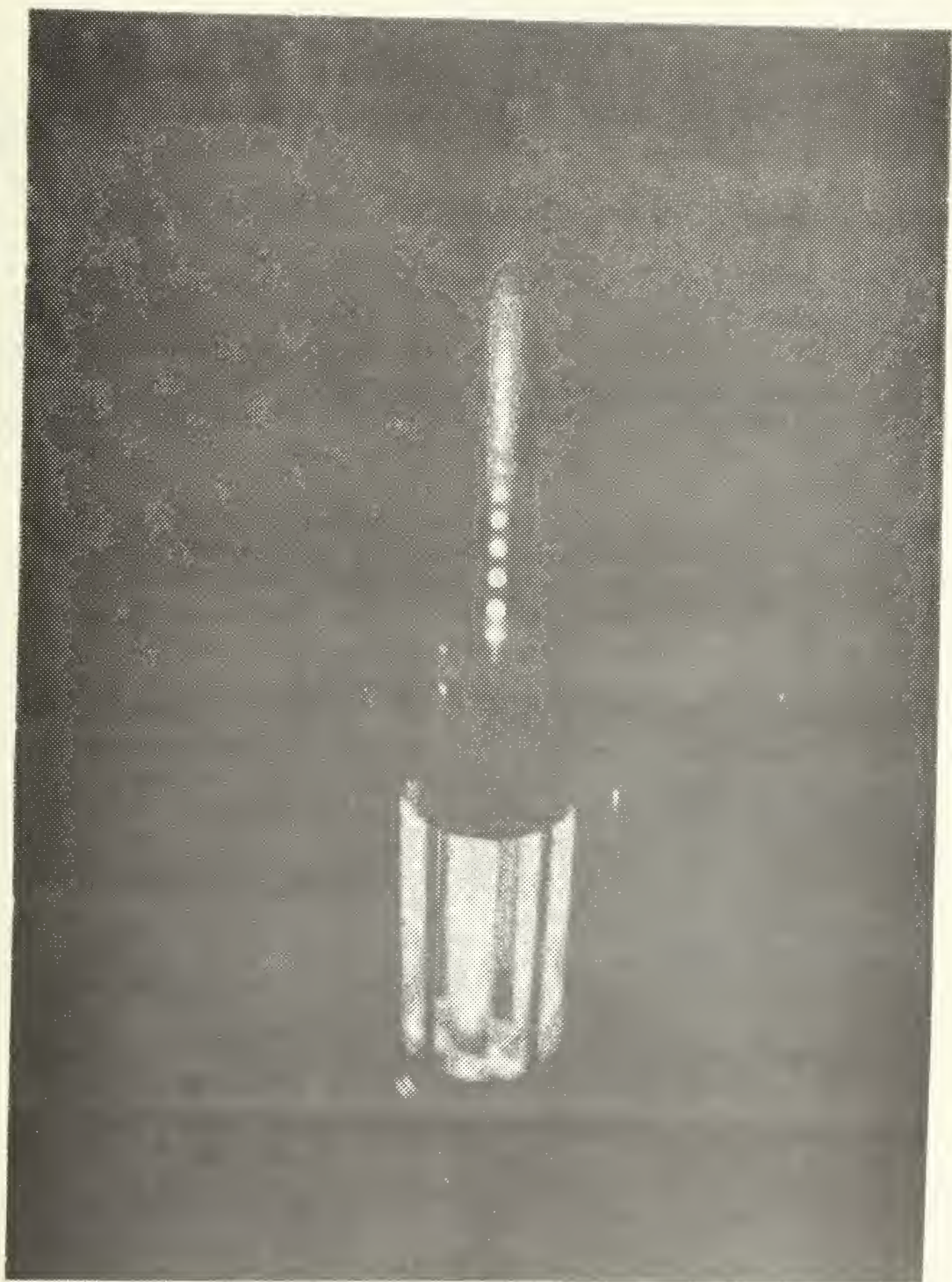


FIGURE 7. TEST STAND



FIGURE 8. RAMJET MOTOR FIRING





NORTH WALL

$$\psi = \psi_{\text{wall}} = \text{constant}$$

$$T = 1$$

STEP WALL

$$\psi = \psi_{\text{wall}} = \text{constant}$$

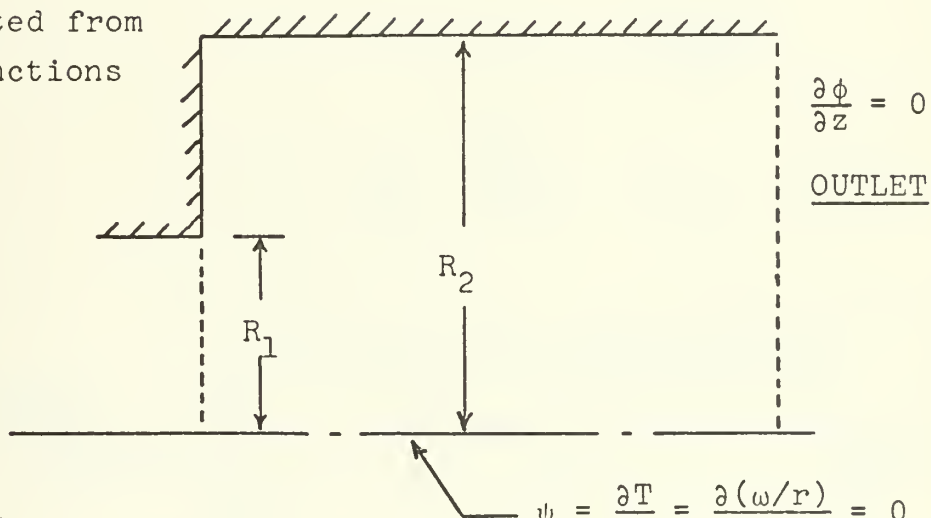
$$v_r = v_z = 0$$

$$\frac{\partial T}{\partial z} = 0$$

$\omega/r, k, \epsilon$  calculated from  
wall functions

$$\omega/r, k, \epsilon$$

calculated from  
wall functions



INLET

$$v_z = v_{\text{in}} = \text{constant}$$

$$\psi \text{ from } \frac{\partial \psi}{\partial r} = \rho r v$$

$$\omega/r = 0$$

$$k = 0.004 v_{\text{in}}^2$$

$$\epsilon = k_{\text{in}}^{3/2} / \ell$$

$$\ell = 0.05 R_2 (0.22)$$

$$T = 0$$

$$T = \frac{t - t_{\text{inlet}}}{t_{\text{wall}} - t_{\text{inlet}}}$$

FIGURE 9. BOUNDARY CONDITIONS FOR PISTEP II  
(Figure 2 from Ref. 15)



NORTH WALL

$$FAR = \frac{\dot{M}_{wall}}{\dot{M}_{in}}$$

$$\dot{M}_{wall} = 2\pi R_2 L \rho V_r$$

$$V_r = \frac{FAR R_1^2 V_{in}}{2 R_2 L}$$

$$\psi = \psi_{wall} + \frac{\dot{M}_{wall} z}{2\pi L}$$

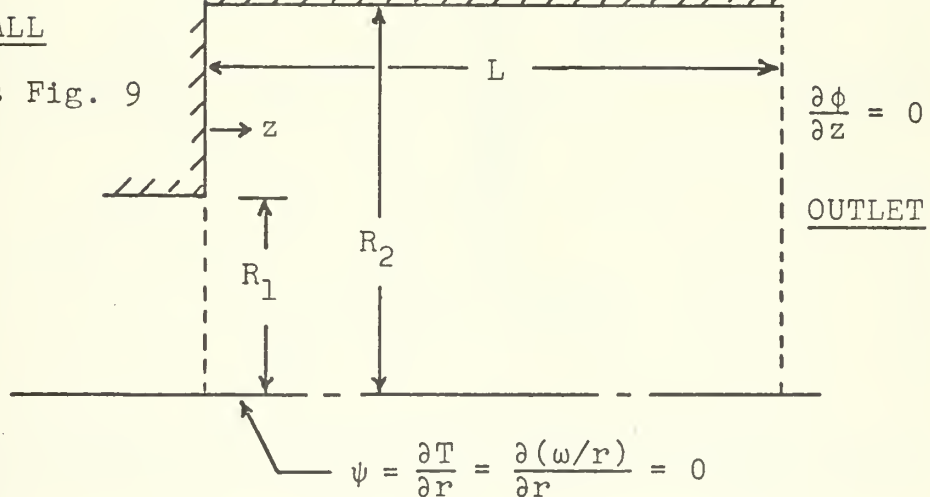
$$\frac{\partial \psi}{\partial z} = \frac{\dot{M}_{wall}}{2\pi L} = \rho R_2 V_r = \text{constant}$$

$$T = 1$$

$\omega/r, k, \epsilon$  - wall functions

STEP WALL

Same as Fig. 9



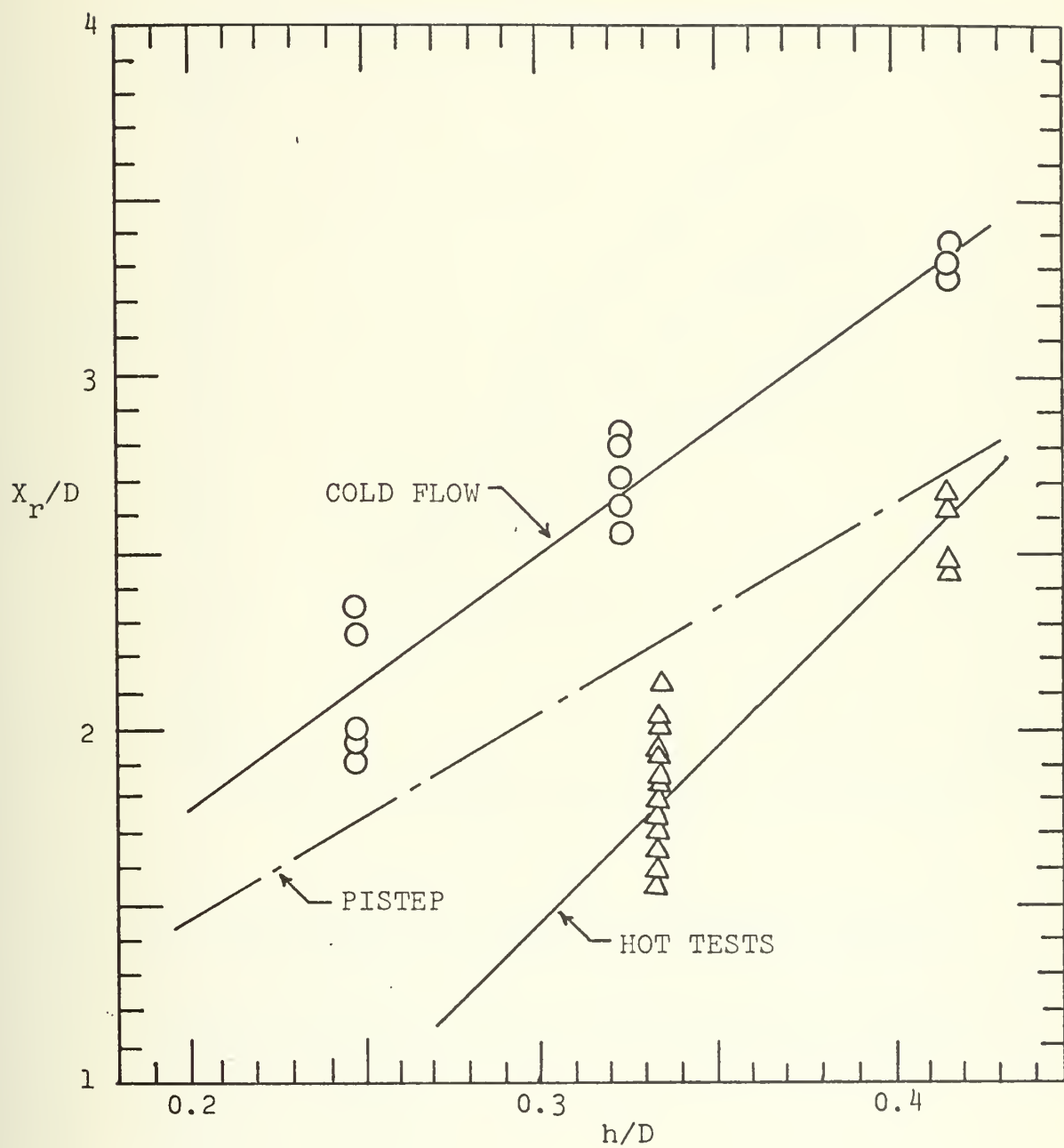
INLET

Same as Fig. 9

$$T = \frac{t - t_{inlet}}{t_{wall} - t_{inlet}}$$

FIGURE 10. BOUNDARY CONDITIONS WITH WALL MASS INJECTION



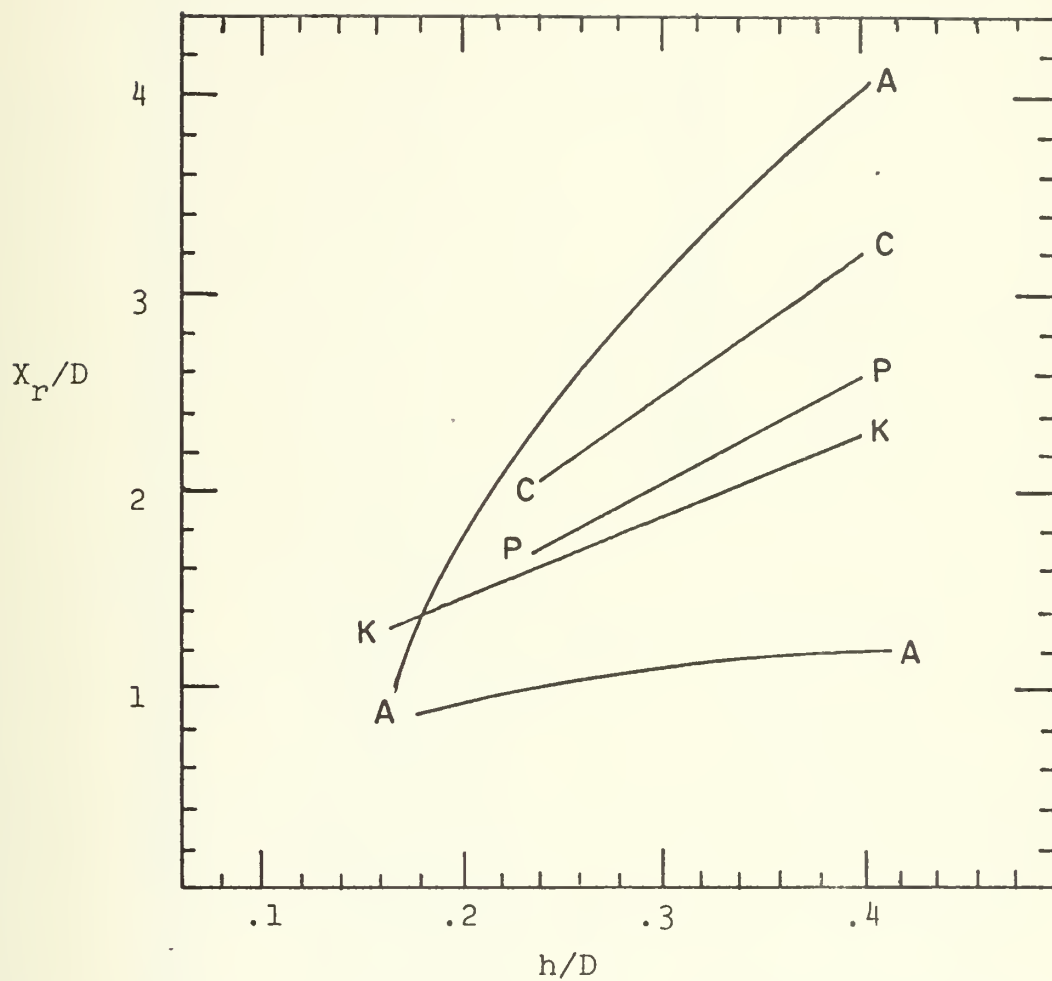


$$\text{COLD FLOW: } X_r/d = 7.15(h/D) + 0.35$$

$$\text{PISTEP: } X_r/d = 5.54(h/D) + 0.36$$

FIGURE 11. REATTACHMENT POINT VS. STEP HEIGHT





K—K Krall and Sparrow - based on location of maximum heat transfer coefficient (axisymmetric flow)

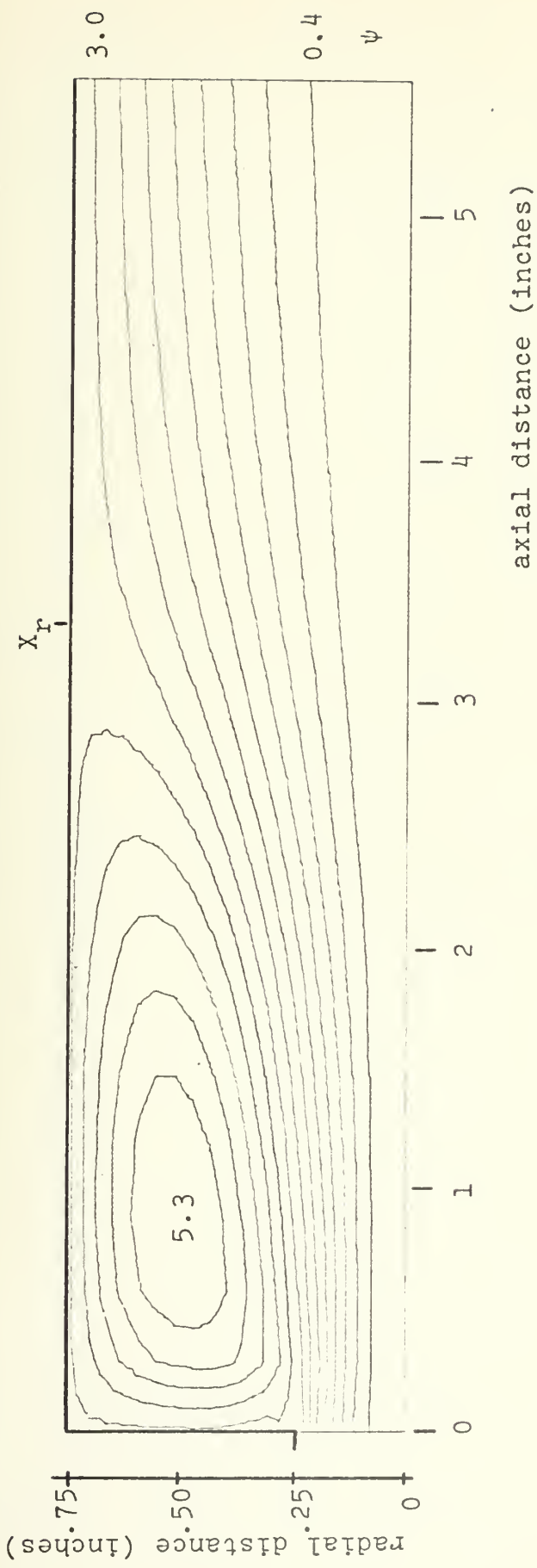
A—A Abbott and Kline - note different reattachment point locations for each side of two-dimensional channel

C—C COLD FLOW RESULTS

P—P PISTEP II RESULTS

FIGURE 12. REATTACHMENT POINT DATA COMPARISON





VIN = 15240

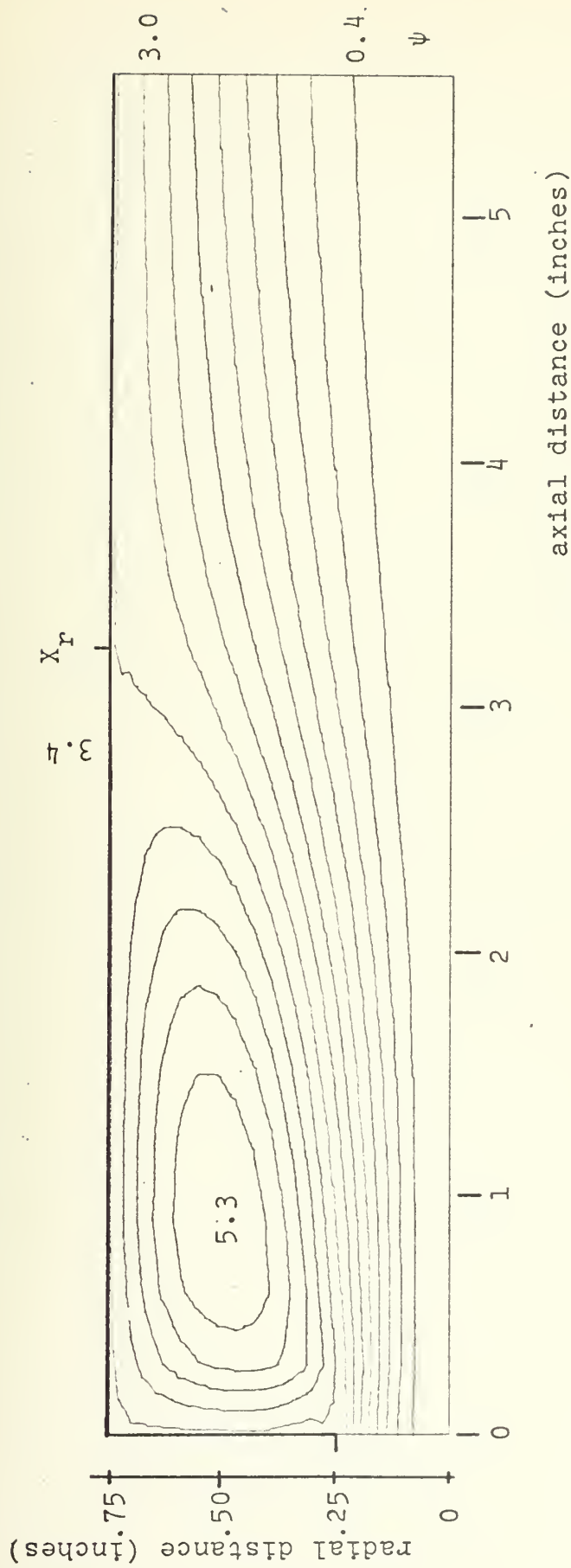
h/D = 0.342

$X_r/D = 2.211$

FAR = 0.0

FIGURE 13. STREAMLINES FOR NON-REACTING FLOW

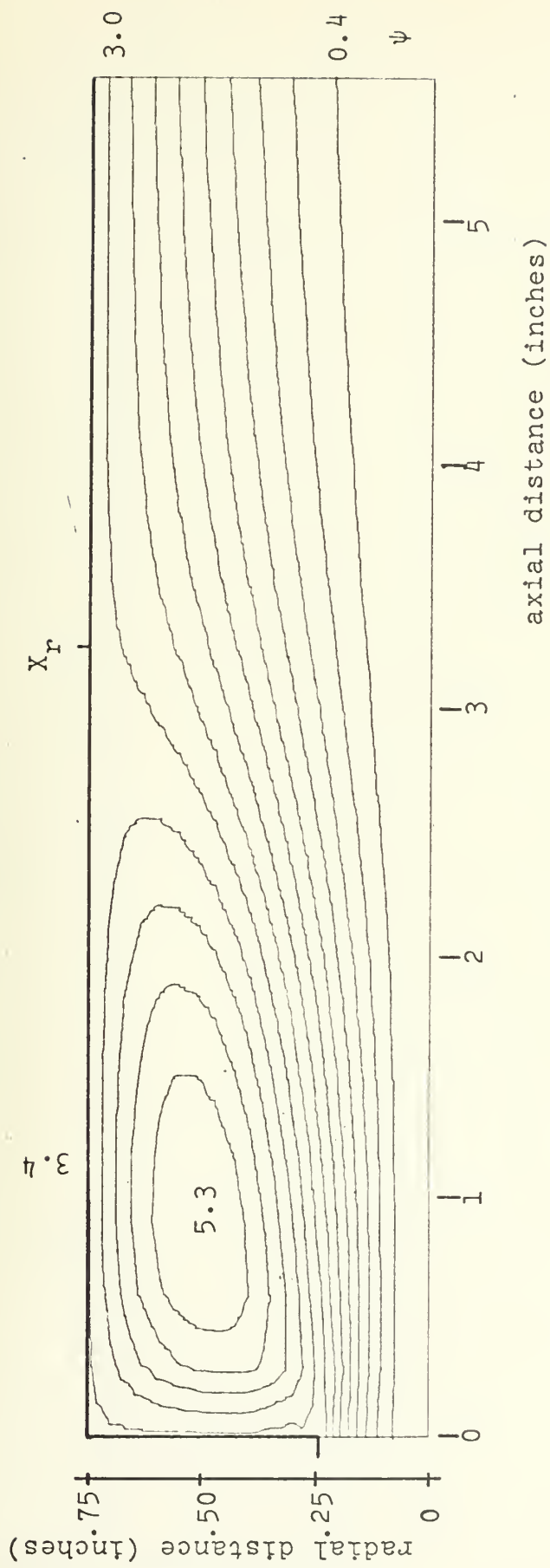




$V_{IN} = 15240$   
 $h/D = 0.342$   
 $X_r/D = 2.191$   
 $FAR = 0.1$

FIGURE 14. STREAMLINES FOR NON-REACTING FLOW

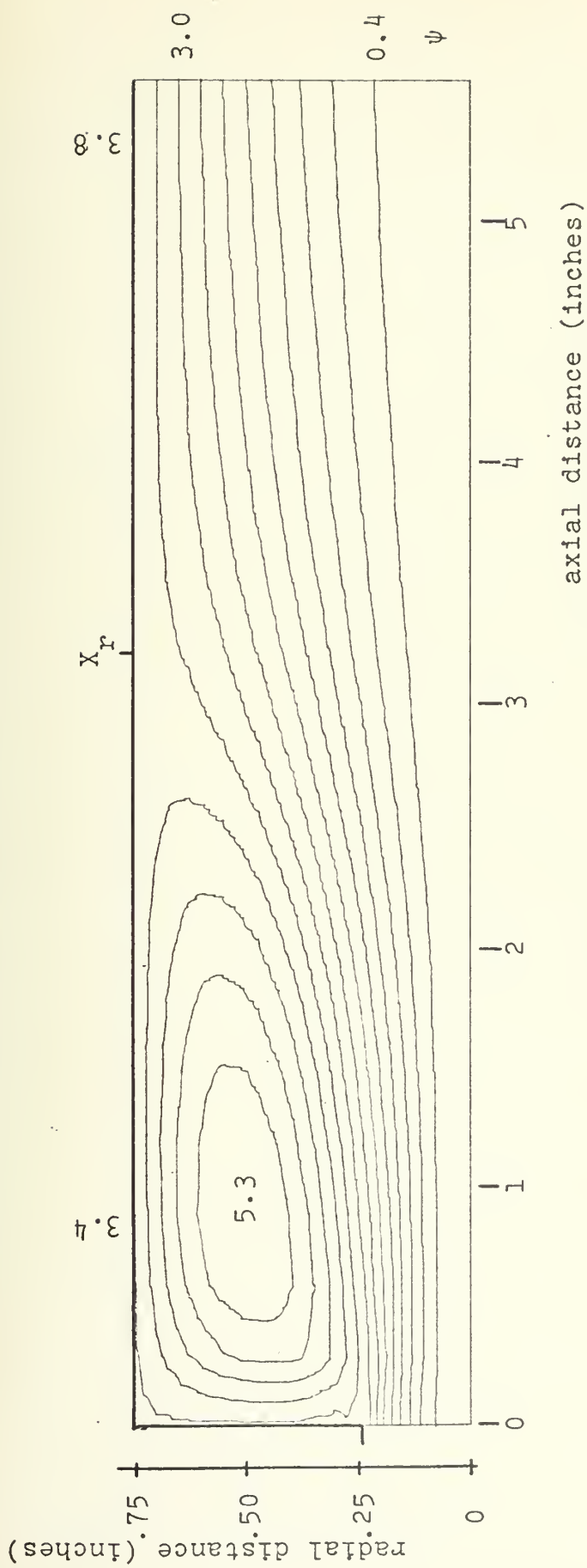




$V_{IN} = 15240$   
 $h/D = 0.342$   
 $X_r/D = 2.168$   
 $FAR = 0.2$

FIGURE 15. STREAMLINES FOR NON-REACTING FLOW

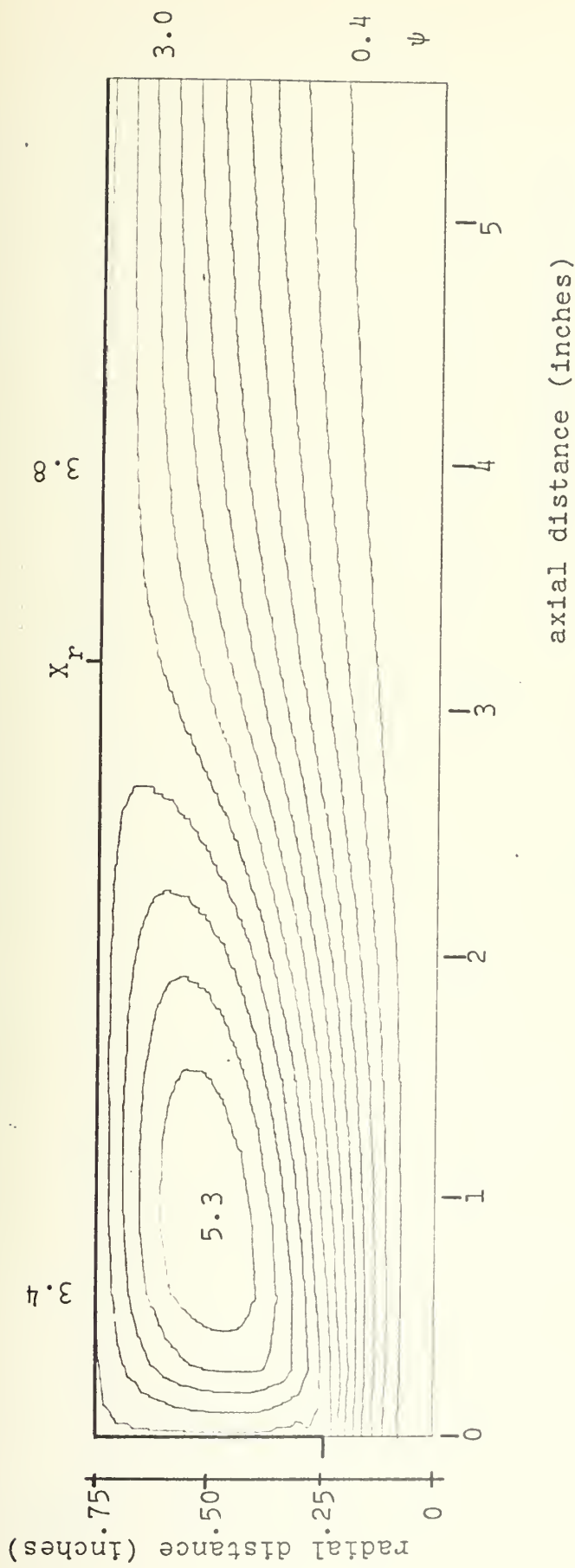




$VIN = 15240$   
 $h/D = 0.342$   
 $X_r/D = 2.145$   
 $FAR = 0.3$

FIGURE 16. STREAMLINES FOR NON-REACTING FLOW

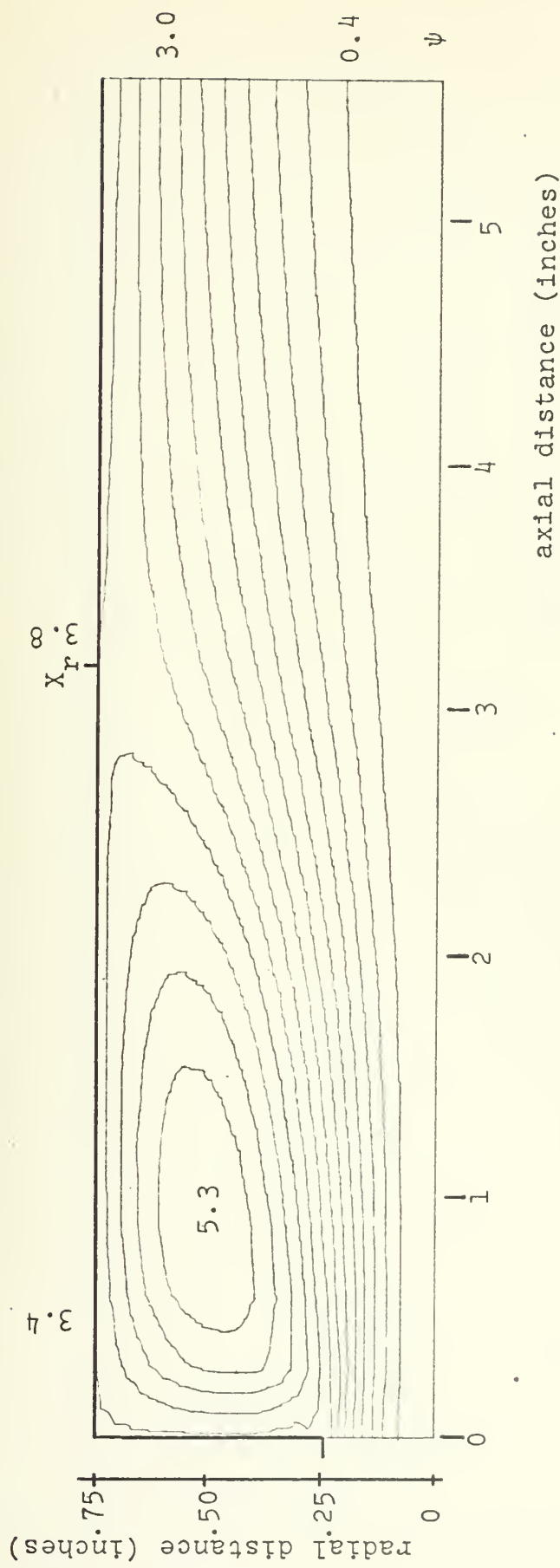




$VIN = 15240$   
 $h/D = 0.342$   
 $X_r/D = 2.123$   
 $FAR = 0.4$

FIGURE 17. STREAMLINES FOR NON-REACTING FLOW

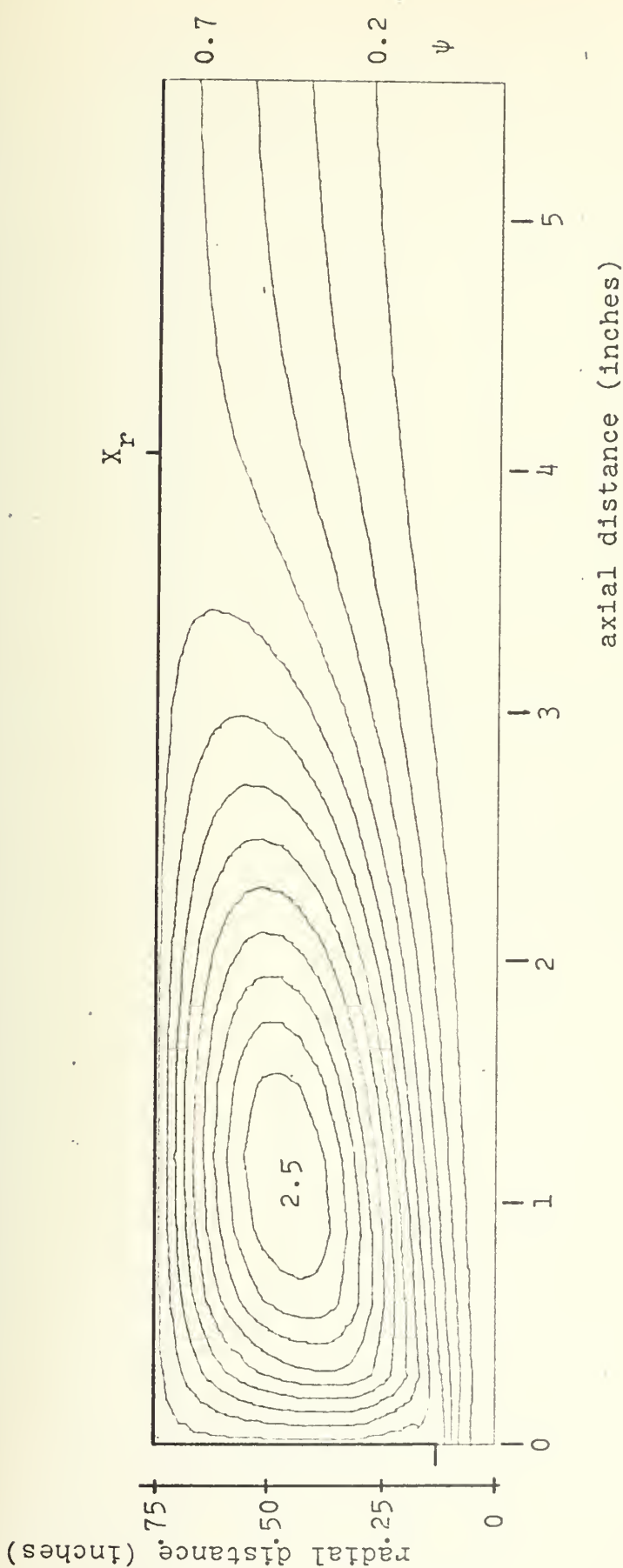




$V_{IN} = 15240$   
 $h/D = 0.342$   
 $X_r/D = 2.101$   
 $FAR = 0.5$

FIGURE 18. STREAMLINES FOR NON-REACTING FLOW





VIN = 15240

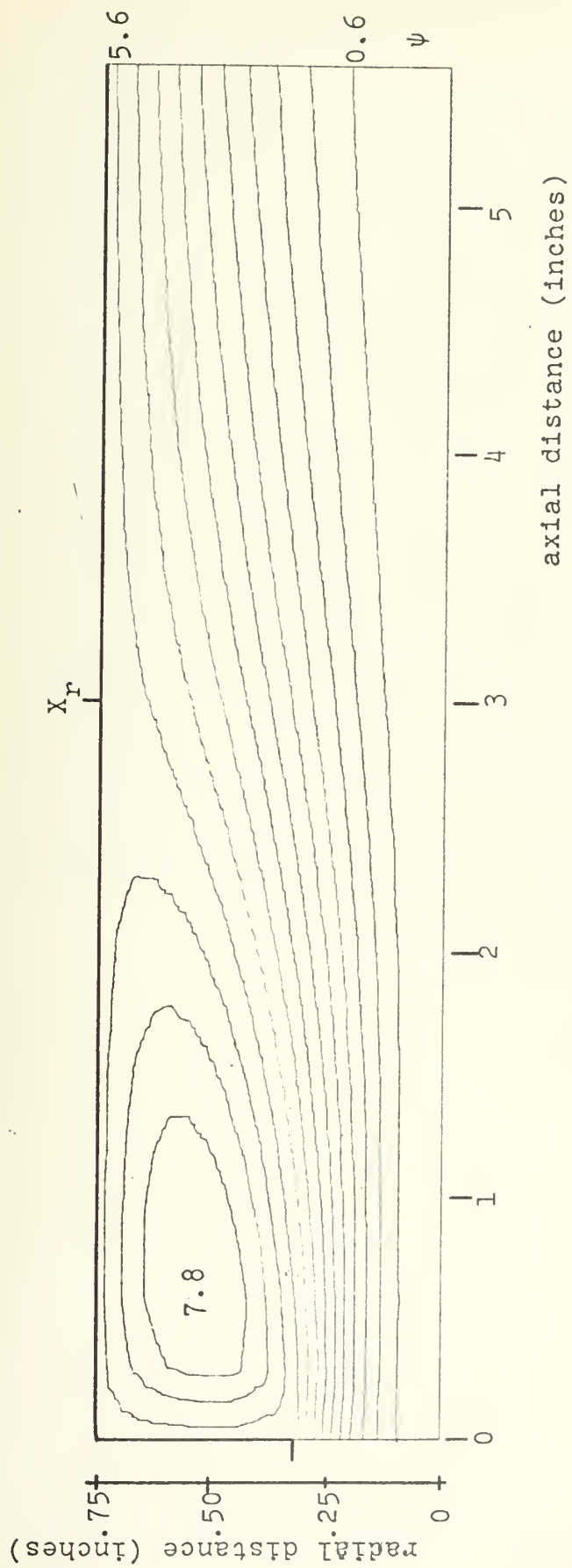
h/D = 0.421

$X_r/D = 2.705$

FAR = 0.0

FIGURE 19. STREAMLINES FOR NON-REACTING FLOW

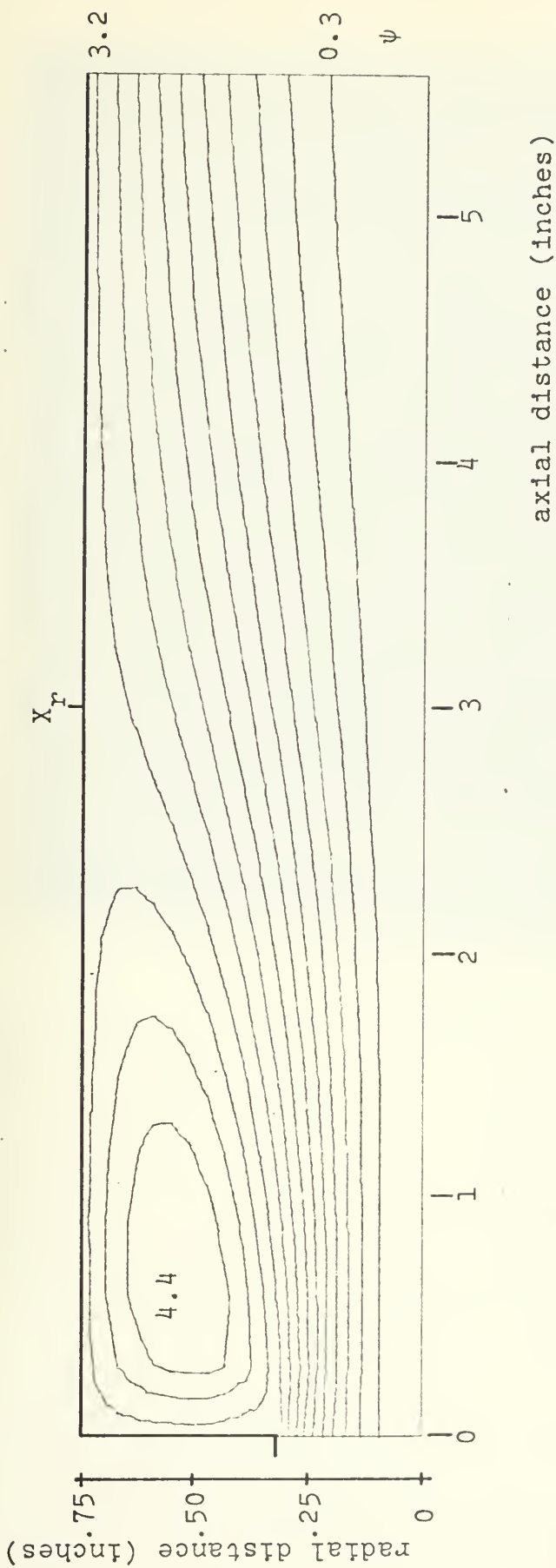




$VIN = 15240$   
 $h/D = 0.289$   
 $X_r/D = 2.002$   
 $FAR = 0.0$

FIGURE 20. STREAMLINES FOR NON-REACTING FLOW

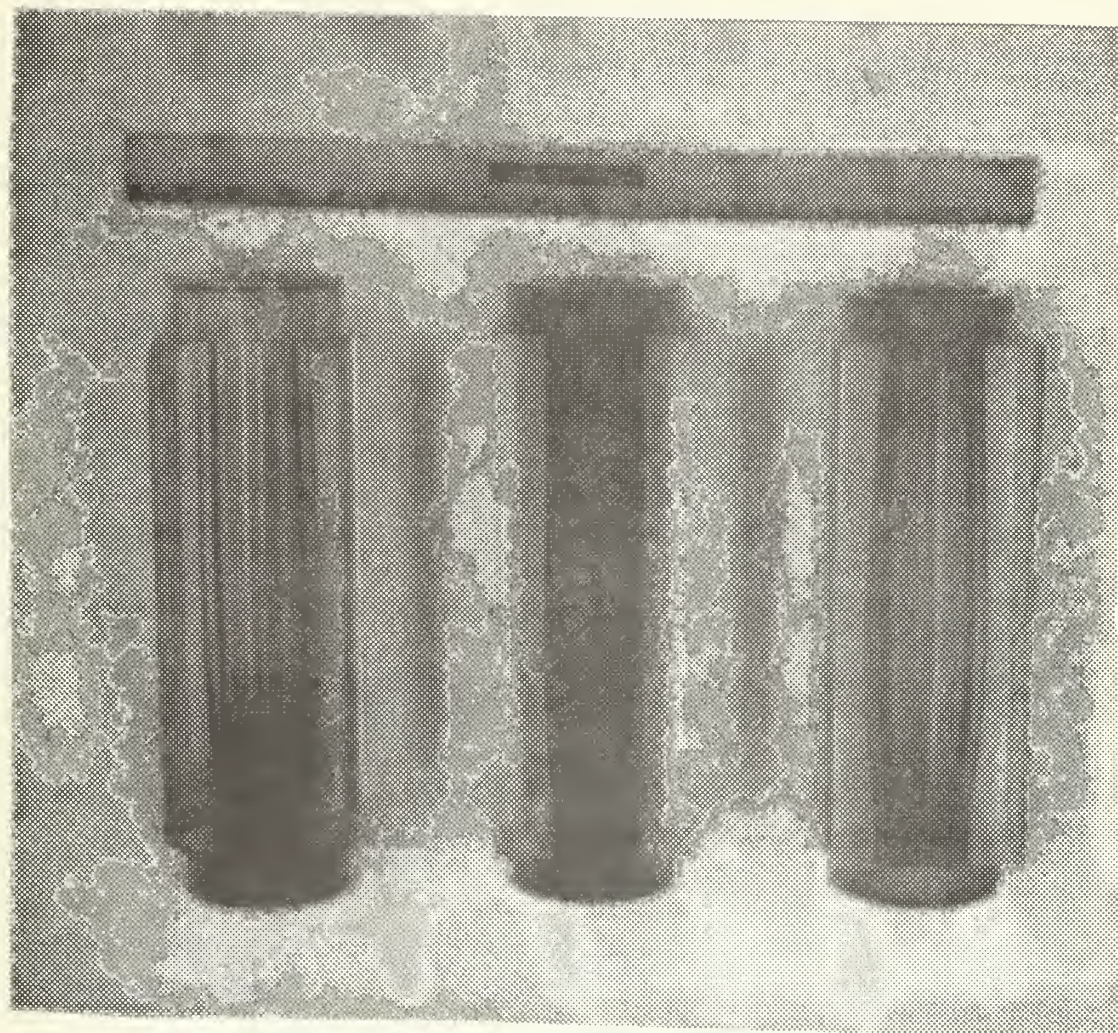




$VIN = 8573$   
 $h/D = 0.289$   
 $X_r/D = 1.999$   
 $FAR = 0.0$

FIGURE 21. STREAMLINES FOR NON-REACTING FLOW





TEST	15	74	60
$h/D$	.33	.33	.41
$P_c$	62	55	71
$T_{in}$	66	320	203
$G_{air}$	.244	.074	.068
$W_{air}$	.43	.13	.12

FIGURE 22. REGRESSION PATTERNS



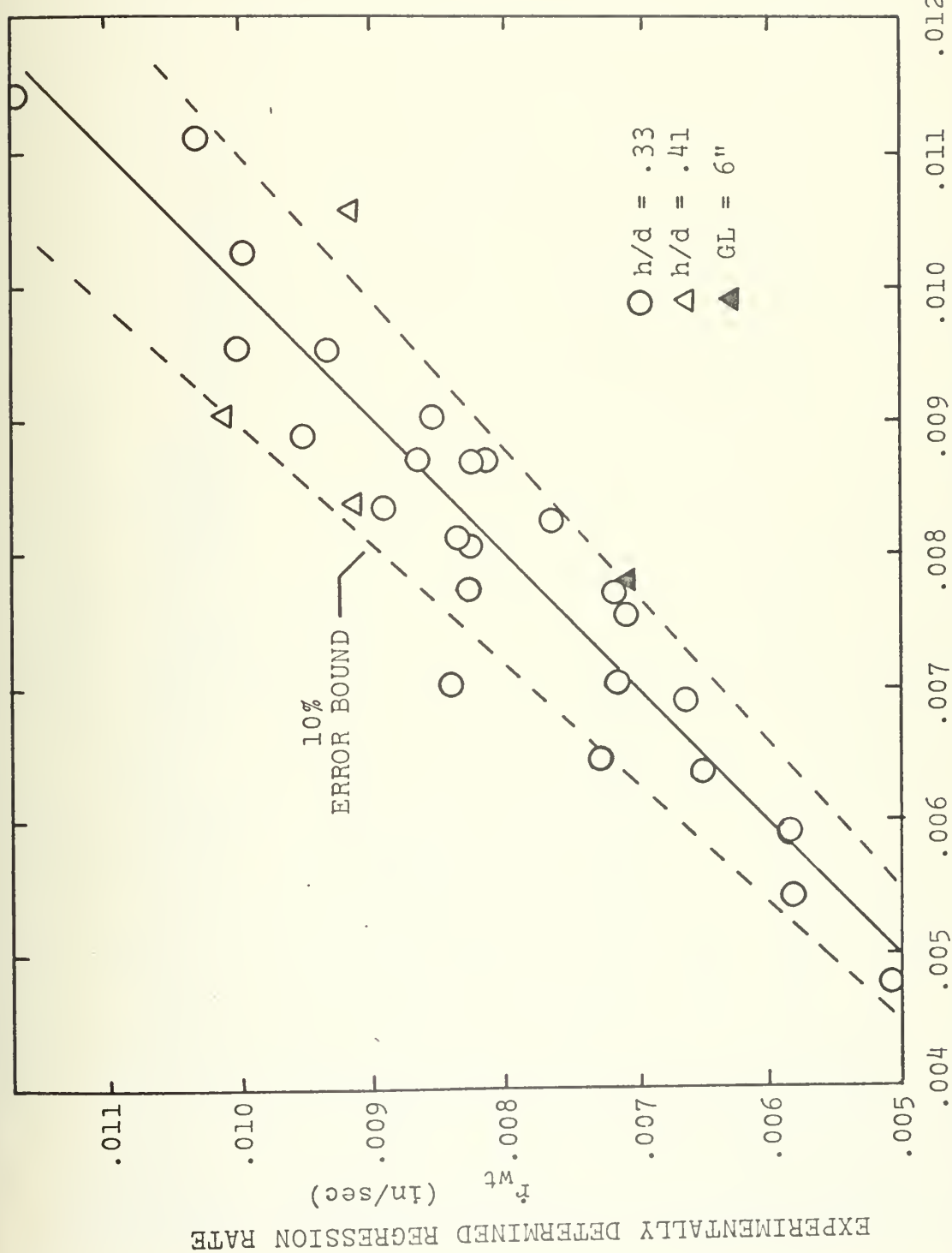


FIGURE 23. EMPIRICAL REGRESSION RATE EQUATION



## APPENDIX A: PROGRAM TO CONTOUR STREAMLINES

```

C COMPUTER PROGRAM TO TRANSFORM AND CONTOUR THE STREAM
C FUNCTIONING OUTPUT FROM PISTEP II FOR VARIOUS WALL
C BLOWING RATES ••••• BY L.D. BOAZ.
C DIMENSION AM(20,20),CL(15),AC(20,20)
C DIMENSION X(20,20),Y(20,20),XIU(20,20)
C DIMENSION AA(20,20),V(20,20),YY(20,20),YI(20,20)
C REAL*8 AA, V, YY, YI
C REAL*8 PTITLE(12), STREAML, INES, FOR, COLD, FL, OW, IN, SO, LID
C FUEL, RAMJET, L.D. BOAZ, Z, REAT, TACHMENT, X/D=1.99, X/D=1.99
C FARE=0
C LOGICAL LTG(3)
C
C 12 LOGICAL LTG(3)
C
C 501 DO 501 I=1,20
C      READ(5,500)(A(I,J),J=1,10)
C 502 DO 502 I=1,20
C      READ(5,500)(A(I,J),J=11,20)
C      READ(5,500)(X1(I,J),J=11,20)
C      READ(5,500)(X2(I,J),J=11,20)
C      READ(5,500)(X2(J,J),J=11,20)
C
C 500 FORMAT(10F8.4)
C      READ(5,510) XRD, FAR
C 510 FORMAT(2F8.4)
C      DO 10 I=1,20
C      U(I)=DBLE(X1(I))
C      V(I)=DBLE(X2(I))
C 10  AA(I,J)=DBLE(A(I,J))
C      DO 10 I=1,20
C      AA(I,J)=DBLE(A(I,J))
C      XIU(1)=0.
C      DX1=X1(16)/19.
C      DO 20 I=2,20
C      XIU(I)=XIU(I-1)+DX1
C      X2U(1)=0
C      DX2=X2(20)/19.
C      DO 21 I=2,20
C      X2U(I)=X2U(J-1)+DX2
C      DO 30 I=1,20
C      X=DBLE(X1U(I))
C      Y=DBLE(X2U(I))
C      N=20
C      DO 40 NR=1,N
C      DO 41 NC=1,M
C 41  YY(NC)=AA(NR,NC)
C      CALL SPLIN1(V,YY,M,Y,YI(NR))

```



```
CALL SPLIN1(U,YI,N,X,FXY)
AC(I,J)=SNGL(FXY)
```

```
30 CONTINUE
IN=20
JN=20
101 WRITE(6,101)(X1(J),J=1,JN)
102 FORMAT(25HODISTANCES IN DIRECTION-1/(1H ,1P5E15.3))
103 FORMAT(25HODISTANCES IN DIRECTION-2/(1H ,1P5E15.3))
104 FORMAT(6:104,"THE DISTRIBUTION OF STREAM FUNCTION FROM P1STEP II
1.0*NON-UNIFORM GRID./")
105 FORMAT(6:105,"THE DISTRIBUTION OF STREAMFUNCTION WITH A UNIFORM GRID
1.0*")
106 CALL PRINT(AC,IN,JN)
DO 300 I=1,IN
DO 300 J=1,JN
107 I=IN-I+1
108 AM(I,J)=AC(J,II)
300 CONTINUE
109 WRITE(6,105) XRD,FAR
110 FORMAT(10.1,105) XRD,FAR= F8.4,5X,FAR=F8.4/
111 CALL CONTR(AM,20,20,20,CL,-15,PTITLE,8,2,LTG)
112 STOP
END
```

```
SUBROUTINE PRINT (A,IN,JN)
DIMENSION A(20,20)
IA=IN/1
112 IB=1,IA
113 IC=(IB-1)*11+1
114 ID=IB+1
DO 115 L=1,JN
115 L=1,JN
J=JN-L+1
116 WRITE(6,101) J,(A(I,J),I=IC,1D)
CONTINUE
117 WRITE(6,103) (I,I=IC,1D)
118 IF((ID*EQ*1N) GO TO 111
119 IF((JN*GT*21) WRITE(6,105)
CONTINUE
120 L=1,JN
121 ID=ID+1
DO 122 L=1,JN
J=JN-L+1
```



```

20
      WRITE(6,111) J, (A(I,J), I=1E, IN)
      CCNTINUE
      WRITE(6,113) (I,I=1E, IN)
      CCNTINUE
      FORMAT(1H 12,5X,1P11E11.3)
      FORMAT(1H0,3X,1I(9X,12)7)
      FORMAT(1H045X,28HCONTINUED IN THE
      FORMAT(1H145X,28HCONTINUED IN THE
      FORMAT(1H 12,5X,1P10E11.3)
      FORMAT(1H0,3X,10(9X,12))
      RETURN
      END
111
1103
104
105
111
113

```

## SUBROUTINE SPLIN

PURPOSE PROVIDES INTERPOLATED VALUE USING "CUBIC SPLINE FITTING"

USAGE FIRST CALL TO SUBROUTINE:  
CALL SPLIN (X,Y,M,XINT,YINT)

```
SUBSEQUENT CALLS:
CALL SPLINN(X,Y,M,XINT,YINT)
```

DESCRIPTION OF PARAMETERS  
 X: MONOTONICALLY INCREASING ABSISSA ARRAY  
 Y: ONE-FOR-ONE CORRESPONDING ORDINATE ARRAY  
 M: NUMBER OF X AND Y VALUES SUPPLIED < OR = 400  
 XINT: VALUE OF ABSISSA FOR WHICH CORRESPONDING ORDINATE  
 YINT: IS TO BE INTERPOLATED (OR EXTRAPOLATED)  
 YINT: INTERPOLATED (OR EXTRAPOLATED) ORDINATE VALUE

X, Y, XINT, AND YINT ARE REAL #8

REMARKS  
IF SPECIFIED X FALLS OUTSIDE OF RANGE, AN EXTRAPOLATED  
VALUE WILL BE SUPPLIED

SUBROUTINES AND FUNCTION SUBROUTINES INCLUDED IN SUBROUTINE SPLICO

MATHEMATICAL METHOD  
UPON FIRST ENTRY TO SPLIN, A CALL TO SPLICO IS MADE TO  
DETERMINE THE COEFFICIENTS TO BE USED IN PERFORMING THE  
INTERPOLATIONS. SEARCH FOR BRACKETING ABSOLUTE VALUES IS  
ALWAYS MADE FROM THE REFERENCE LAST USED IN INTERPOLATING.



SAMPLE PROGRAMS

1. GIVEN 10 PAIRS OF ABSISSA AND ORDINATE VALUES:

```
X=1.5, 15, 21, 25, 32, 38, 44, 75, 90.  
Y=0, 50, 250, 400, 750, 780, 900, 950, 975, 1100.
```

FIND AN ORDINATE VALUE WHEN THE ABSISSA VALUE IS:  
20., 60., AND 100.

```
REAL*8 X(10), Y(10), XINT(3)/20.60./, YINT(3)  
CALL SPLIN(X,Y,10,XINT(1),YINT(1))  
DO 20 I=2,3  
20 CALL SPLIN(X,Y,10,XINT(I),YINT(I))
```

2. GIVEN A TWO DIMENSIONAL TABLE WITH N ROWS AND M COLUMNS,  
N ABSISSA VALUES, AND M ORDINATE VALUES, DETERMINE A  
VALUE IN THE TABLE AT A SPECIFIED ABSISSA AND ORDINATE  
VALUE.

```
REAL*8 A(10,20), U(10), V(20), YY(10), YI(10), X, Y, FXY  
N=10  
M=20  
DO 100 NR=1,N  
DO 101 NC=1,M  
101 YY(NC)=A(NR,NC)  
100 CALL SPLIN(V,YY,M,Y,YI(NR))  
CALL SPLIN(U,YI,N,X,FXY)
```

WHERE N IS THE NUMBER OF ROWS IN A  
M IS THE NUMBER OF COLUMNS IN A  
U CONTAINS THE N ABSISSA VALUES  
V CONTAINS THE M ORDINATE VALUES  
YY CONTAINS A SELECTED ROW OF THE TABLE A  
YI CONTAINS AN INTERPOLATED VALUE OF A FOR EACH ROW  
X IS THE ABSISSA FOR WHICH A FUNCTION VALUE  
Y IS THE ORDINATE FOR WHICH A FUNCTION VALUE IS  
FXY IS A VALUE OF A AT X, Y



```

SUBROUTINE SPLIN1(X,Y,M,XINT,YINT)
IMPLICIT REAL*8 (A-H),Y(M),C(4,400)
DIMENSION X(M),Y(M),C(4,400)
CALL SPLICO(X,Y,M,C)
K=1
ENTRY SPLINN(X,Y,M,XINT,YINT)
3 IF(XINT-X(1))70,1,2
 1 K=1
 2 GO TO 7
 3 YINT=Y(1)
 4 RETURN
 5 YINT=X(K+1)
 6 RETURN
 7 K=M-1
 8 IF(M-K)71,71,3
 9 K=M-1
10 GO TO 7
11 YINT=Y(K)
12 RETURN
13 K=M-1
14 GO TO 6
15 PRINT 101,XINT
16 FCNAT(8H0,XINT=E18.9,32H,OUT OF RANGE FOR INTERPOLATION)
17 YINT=(X(K+1)-XINT)*(C(1,K)*(X(K+1)-XINT)**2+C(3,K))
18 YINT=YINT+(XINT-X(K))*(C(2,K)*(XINT-X(K))**2+C(4,K))
19 RETURN
20 END

SUBROUTINE SPLICO(X,Y,M,C)
IMPLICIT REAL*8 (A-H),Y(M),C(4,400)
DIMENSION X(M),Y(M),C(4,400)
12(400)
1 MN=M-1
2 DO 2 K=1,MN
3 D(K)=X(K+1)-X(K)
4 P(K)=D(K)/6.
5 E(K)=(Y(K+1)-Y(K))/D(K)
6 DO 3 K=2,MN

```



```

3 B(K)=E(K)-E(K-1)
A(1,2)=-1*D(1)/D(2)
A(1,3)=D(1)/D(2)
A(2,3)=P(2)-P(1)*A(1,3)
A(2,2)=2*(P(1)+P(2))-P(1)*A(1,2)
A(2,3)=A(2,3)/A(2,2)
B(2)=B(2)/A(2,2)
DO 4 K=3,M
A(K,2)=2*(P(K-1)+P(K))-P(K-1)*A(K-1,3)
B(K)=B(K)-P(K-1)*B(K-1)
A(K,3)=P(K)/A(K,2)
A(K,2)=B(K)/D(M-1)
Q=D(M-2)/D(M-1)
A(M,1)=1+Q+A(M-2,3)
A(M,2)=-Q-A(M,1)*A(M-1,3)
B(M)=B(M-2)-A(M,1)*B(M-1)
Z(N)=B(M)/A(M,2)
MN=M-2
DO 6 I=1,MN
K=M-1
Z(K)=B(K)-A(1,2)*Z(2)-A(1,3)*Z(3)
DO 7 K=1,M
Q=1./((6*D(K))
C(1,K)=Z(K)*Q
C(2,K)=Z(K+1)*Q
C(3,K)=Y(K)/D(K)-Z(K)*P(K)
C(4,K)=Y(K+1)/D(K)-Z(K+1)*P(K)
END
7 RETURN

```



## APPENDIX B: RAMJET DATA REDUCTION

COMPUTER PROGRAM TO REDUCE DATA FROM SOLID FUEL RAMJET RUNS  
 BY L. D. BOAZ  
 THE PARAMETERS IN THE PROGRAM ARE:  
 AF • • • AIR FLOW COEFFICIENT  
 AS • • • ASME FLOW COEFFICIENT  
 BP • • • NOZZLE THROAT AREA  
 CC • • • BAROMETRIC PRESSURE  
 CC\*E • • • BAROMETRIC PRESSURE REGRESSION RATE EQUATION  
 D • • • ORIFICE DIAMETER  
 DEF • • • FINAL EXIT DIAMETER  
 DEI • • • INITIAL EXIT DIAMETER  
 DP • • • DP C • • • DP NM • • • DP MM • • • DP IN<sup>1/4</sup>\*3  
 DS • • • DENSITY  
 DST • • • DIAMETER OF THE STEP HOLE  
 ERR • • • DIAMETER ERROR BETWEEN RWT AND EMPIRICAL EQUATION  
 FG • • • FG ISP • • • FG AIR • • • FG GM • • • FG GN • • • FG STEP  
 G • • • SPECIFIC FLUX OF AIR  
 GM • • • MASS ATTENUE LENGTH  
 GN • • • GRAIN NUMBER  
 HD • • • STEP HEIGHT  
 NTOT • • • TOTAL NUMBER OF DATA POINTS TO READ IN  
 NP • • • STEP HEIGHT OF PRESSURE  
 PC • • • CHAMBER PRESSURE  
 RDE • • • REGRESSION RATE BASED ON EXIT DIAMETER  
 RFST • • • REGRESSION NUMBER BASED ON ORIFICE DIAMETER  
 RT • • • REGRESSION RATE WITH AIR NUMBER  
 RWT • • • REGRESSION RATE BASED ON WEIGHT  
 SFC • • • SPECIFIC FUEL CONSUMPTION  
 STC • • • ORIFICE TEMPERATURE  
 TIGA • • • CHAMBER TEMPERATURE WITH METHANE  
 TTIGA • • • TOTAL IGNITION TIME INTO RUN  
 TTIN • • • IGNITION TEMPERATURE INTO CHAMBER  
 TTUM • • • TOTAL METHANE-<sup>OX</sup> (ONLY) TIME, INCLUDING MISFIRES  
 UPO • • • MEAN CHAMBER VELOCITY  
 VIS • • • VISCOSITY  
 WDDT • • • WEIGHT FLOW RATE OF AIR







```

606 FORMAT('1'//'/','INPUT DATA')
611 WRITE(6,1)
1 FORMAT('0',T21,'TEST#',T28,'IG-TIME',T37,'REAT-PT',T47,'CHAMBER'
2 PC NOISE, T66,NOZZLE,T74,INITIAL,T84,FINAL,T92,STEP
3 /T27,INTORUN,T39,(IN),T47,P(PSIG),T57,(PSIA),T66,D*(1
3N),T74,WT(GM),T83,WT(GM),T93,(IN),/)

DO 240 N=1,NTOT
240 WRITE(6,621) TEST(N),TIGA(N),XR(N),PC(N),DPC(N),DS(N),WTI(N),
1 WTF(N),H(N)
1 FORMAT('T22,I2,T29,F5.3,T39,F4.2,T48,F5.1,T58,F5.2,T66,F5.3,T74
1 F6.1,T83,F6.1,T93,F5.3)
1 WRITE(6,606)
1 WRITE(6,612)
1 FORMAT(DSTEP,T21,'TEST#',T28,'INITIAL',T37,'FINAL',T44,'GR.LENGTH',
1 T55,DSTEP,T65,TM,T28,D(IN),T37,D(IN),T46,(IN),T56,
2 (IN),T63,(SEC),//)
2 DO 245 N=1,NTOT
245 WRITE(6,622) TEST(N),DEF(N),GL(N),DSTEP(N),TM(N)
622 FORMAT(6,22,I2,T28,I2,T28,F5.3,T37,F5.3,T45,F6.3,T55,F5.3,T63,F5.2)
DD=2.46
DO 210 N=1,NTOT
210 BP(N)=BP(N)+BP(N)
P(N)=P(N)+BP(N)
PC(N)=PC(N)+BP(N)
TC(N)=T(N)+459.67
TIN(N)=TIN(N)+459.67
VIS=.0001241*(T(N)/540.0)**0.72253
CALCULATE RED BY NLDSDS NUMBER BY GUESSING THE FLOW RATE.
WDOT(N)=2.5*WDOT(N)/VIS
RED=6.210925*WDOT(N)/VIS
BETA=D(N)/DD
X=DBLE(BETA)
Y=DBLE(RED)
NN=10
M=7
DO 110 NR=1,NN
110 DO 111 NC=1,M
111 YY(NC)=A(NR,NC)
CALL SPLINI(U,YY,M,YI(NR))
CALL SPLINI(U,YI,NN,X,FXY)
CK=SNGL(FXY)
YF=1.0-(0.41+(0.35*(BETA**4.0))**DP(N))**4*P(N)/(DP(N)**F**SQR(D(N))**YF)
WDOT(N)=0.86234829*CK*D(N)*D(N)*YF*SQR(D(N))/VIS
RED=6.210925*WDOT(N)/VIS
Y=DBLE(RED)
DO 120 NR=1,NN
120 DO 121 NC=1,M

```



```

121 YY(NC)=A(NR,NC)
120 CALL SPLINI(V,YY,M,YI(NR))
CALL SPLINI(U,YI,NN,X,FXY)
CK=SNGL(FXY)
AK(N)=CK
WDOT(N)=0.86234829*CK*D(N)*D(N)*YF*SQRT(DP(N)*P(N)/T(N))
AS=3.14159*DS(N)*DS(N)/4.0
GM=1.0
R=50.0
WTI(N)=WTI(N)-3*2*TM(N)
WF(N)=((WTI(N)-WTF(N))/RT(N))/453.59237
WTC(N)=((AS*PC(N)/(WDT(N)+WF(N)))*2.0)*(GM*32.174/R)*((2.0/(GM+1.
10))*
1 RDE(N)=(DEF(N)/(GM-1.0))
DPM=19*6405
RWT(N)=(SQR((4.0*(WTI(N)-WTF(N))/(DPMM*GL(N)*3.14159))+DEI(N))
1 DEI(N)=((WF(N)+WDT(N))/((2.0*RT(N))
FG(N)=(BP(N)/PC(N))**SQR((2.0*GC*GM*RT(N)/(GM-1.0))+DEI(N))
1 FIS=(BP(N)/FG(N))**SQR((2.0*GC*GM*RT(N)/(GM-1.0)))/GC
VIS=0.001241*(TIN(N)/540.0)*72253
RESTEP=3.14159*DSTEP(N)/4.0
AFA(N)=WDT(N)/(WF(N)*DEI(N))
AAVE=3.14159*DEI(N)*DEI(N)/4.0
GAI(N)=WDT(N)/AAVE
UPORT(N)=WDT(N)*RT(N)/RT(N)/(PC(N)*AAVE)
HD(N)=H(N)/DEI(N)
XRD(N)=XRD(N)/DEI(N)
SFC(N)=3600.*WF(N)/DEI(N)
EQN(Y)=(PC(N)*0.51)*(TIN(N)*0.34)*(GAI(N)*0.41)
CC(N)=RWT(N)/EQN(N)
210 CONINU
607 WRITE(6,607)/////////T21,'CALCULATED RESULTS'
613 FORMAT(6,6,1,3)
1 T58*PWT,T68*TEST#,T29*WDDT,T37*CHAMBER,T46*CHAMBER,
2 T38*T(R),T46*T79*WF,T87*T96*T27*GLM/SEC),
3 *(LBM/SEC),T95*(LBF)//)
270 WRITE(6,623)TEST(N),WDT(N),PC(N),RWT(N),RDE(N),WF(N),
1 RESTEP(N):FG(N)
623 FORMAT(2T22,I2,T29,F5.3,T37,F6.1,T48,F5.1,T57,F6.4,
2 T78,F6.4,T86,F7.0,T97,F3.0)
WRITE(6,607)
WRITE(6,614)

```







## SOLID FUEL RAMJET DATA REDUCTION

## INPUT DATA

TEST #	GRAIN #	ORIFICE T (F)	ORIFICE P (PSIG)	ORIFICE P (PSI)	DELTA-P (PSI)	BAROMETRIC P (IN.HG.)	INLET T (F)	RUN TIME (SEC)	IGNITION TIME
6	7	118	119	120	212	339	428	492	53
7	8	115	117	118	20	375	387	389	10
2	3	234	57	89	115	117	118	116	116
3	4	5	7	89	213	216	222	225	227
4	5	5	7	89	223	223	223	225	228
5	6	6	6	9	221	221	220	220	229
6	7	6	6	9	219	219	219	219	219
7	8	6	6	9	218	218	218	218	218
8	9	6	6	9	217	217	217	217	217
9	10	6	6	9	216	216	216	216	216
10	11	6	6	9	215	215	215	215	215
11	12	6	6	9	214	214	214	214	214
12	13	6	6	9	213	213	213	213	213
13	14	6	6	9	212	212	212	212	212
14	15	6	6	9	211	211	211	211	211
15	16	6	6	9	210	210	210	210	210
16	17	6	6	9	209	209	209	209	209
17	18	6	6	9	208	208	208	208	208
18	19	6	6	9	207	207	207	207	207
19	20	6	6	9	206	206	206	206	206
20	21	6	6	9	205	205	205	205	205
21	22	6	6	9	204	204	204	204	204
22	23	6	6	9	203	203	203	203	203
23	24	6	6	9	202	202	202	202	202
24	25	6	6	9	201	201	201	201	201
25	26	6	6	9	200	200	200	200	200
26	27	6	6	9	199	199	199	199	199
27	28	6	6	9	198	198	198	198	198
28	29	6	6	9	197	197	197	197	197
29	30	6	6	9	196	196	196	196	196
30	31	6	6	9	195	195	195	195	195
31	32	6	6	9	194	194	194	194	194
32	33	6	6	9	193	193	193	193	193
33	34	6	6	9	192	192	192	192	192
34	35	6	6	9	191	191	191	191	191
35	36	6	6	9	190	190	190	190	190
36	37	6	6	9	189	189	189	189	189
37	38	6	6	9	188	188	188	188	188
38	39	6	6	9	187	187	187	187	187
39	40	6	6	9	186	186	186	186	186
40	41	6	6	9	185	185	185	185	185
41	42	6	6	9	184	184	184	184	184
42	43	6	6	9	183	183	183	183	183
43	44	6	6	9	182	182	182	182	182
44	45	6	6	9	181	181	181	181	181
45	46	6	6	9	180	180	180	180	180
46	47	6	6	9	179	179	179	179	179
47	48	6	6	9	178	178	178	178	178
48	49	6	6	9	177	177	177	177	177
49	50	6	6	9	176	176	176	176	176
50	51	6	6	9	175	175	175	175	175
51	52	6	6	9	174	174	174	174	174
52	53	6	6	9	173	173	173	173	173
53	54	6	6	9	172	172	172	172	172
54	55	6	6	9	171	171	171	171	171
55	56	6	6	9	170	170	170	170	170
56	57	6	6	9	169	169	169	169	169
57	58	6	6	9	168	168	168	168	168
58	59	6	6	9	167	167	167	167	167
59	60	6	6	9	166	166	166	166	166
60	61	6	6	9	165	165	165	165	165
61	62	6	6	9	164	164	164	164	164
62	63	6	6	9	163	163	163	163	163
63	64	6	6	9	162	162	162	162	162
64	65	6	6	9	161	161	161	161	161
65	66	6	6	9	160	160	160	160	160
66	67	6	6	9	159	159	159	159	159
67	68	6	6	9	158	158	158	158	158
68	69	6	6	9	157	157	157	157	157
69	70	6	6	9	156	156	156	156	156
70	71	6	6	9	155	155	155	155	155
71	72	6	6	9	154	154	154	154	154
72	73	6	6	9	153	153	153	153	153
73	74	6	6	9	152	152	152	152	152
74	75	6	6	9	151	151	151	151	151
75	76	6	6	9	150	150	150	150	150
76	77	6	6	9	149	149	149	149	149
77	78	6	6	9	148	148	148	148	148
78	79	6	6	9	147	147	147	147	147
79	80	6	6	9	146	146	146	146	146
80	81	6	6	9	145	145	145	145	145
81	82	6	6	9	144	144	144	144	144
82	83	6	6	9	143	143	143	143	143
83	84	6	6	9	142	142	142	142	142
84	85	6	6	9	141	141	141	141	141
85	86	6	6	9	140	140	140	140	140
86	87	6	6	9	139	139	139	139	139
87	88	6	6	9	138	138	138	138	138
88	89	6	6	9	137	137	137	137	137
89	90	6	6	9	136	136	136	136	136
90	91	6	6	9	135	135	135	135	135
91	92	6	6	9	134	134	134	134	134
92	93	6	6	9	133	133	133	133	133
93	94	6	6	9	132	132	132	132	132
94	95	6	6	9	131	131	131	131	131
95	96	6	6	9	130	130	130	130	130
96	97	6	6	9	129	129	129	129	129
97	98	6	6	9	128	128	128	128	128
98	99	6	6	9	127	127	127	127	127
99	100	6	6	9	126	126	126	126	126
100	101	6	6	9	125	125	125	125	125
101	102	6	6	9	124	124	124	124	124
102	103	6	6	9	123	123	123	123	123
103	104	6	6	9	122	122	122	122	122
104	105	6	6	9	121	121	121	121	121
105	106	6	6	9	120	120	120	120	120
106	107	6	6	9	119	119	119	119	119
107	108	6	6	9	118	118	118	118	118
108	109	6	6	9	117	117	117	117	117
109	110	6	6	9	116	116	116	116	116
110	111	6	6	9	115	115	115	115	115
111	112	6	6	9	114	114	114	114	114
112	113	6	6	9	113	113	113	113	113
113	114	6	6	9	112	112	112	112	112
114	115	6	6	9	111	111	111	111	111
115	116	6	6	9	110	110	110	110	110
116	117	6	6	9	109	109	109	109	109
117	118	6	6	9	108	108	108	108	108
118	119	6	6	9	107	107	107	107	107
119	120	6	6	9	106	106	106	106	106
120	121	6	6	9	105	105	105	105	105
121	122	6	6	9	104	104	104	104	104
122	123	6	6	9	103	103	103	103	103
123	124	6	6	9	102	102	102	102	102
124	125	6	6	9	101	101	101	101	101
125	126	6	6	9	100	100	100	100	100
126	127	6	6	9	99	99	99	99	99
127	128	6	6	9	98	98	98	98	98
128	129	6	6	9	97	97	97	97	97
129	130	6	6	9	96	96	96	96	96
130	131	6	6	9	95	95	95	95	95
131	132	6	6	9	94	94	94	94	94
132	133	6	6	9	93	93	93	93	93
133	134	6	6	9	92	92	92	92	92
134	135	6	6	9	91	91	91	91	91
135	136	6	6	9	90	90	90	90	90
136	137	6	6	9	89	89	89	89	89
137	138	6	6	9	88	88	88	88	88
138	139	6	6	9	87	87	87	87	87
139	140	6	6	9	86	86	86	86	86
140	141	6	6	9	85	85	85	85	85
141	142	6	6	9	84	84	84	84	84
142	143	6	6	9	83	83	83	83	83
143	144	6	6	9	82	82	82	82	82
144	145	6	6	9	81	81	81	81	81
145	146	6	6	9	80	80	80	80	80
146	147	6	6	9	79	79	79	79	79
147	148	6	6	9	78	78	78	78	78
148	149	6	6	9	77	77	77	77	77
149	150	6	6	9	76	76	76	76	76
150	151	6	6	9	75	75	75	75	75
151	152	6	6	9	74	74	74	74	74
152	153	6	6	9	73	73	73	73	73
1									



## INPUT DATA

TEST#	IG. TIME INTO RUN	REAT. PT. (IN)	CHAMBER P (PSIG)	PC NOISE (PSIA)	NOZZLE D* (IN)	INITIAL WT (GM)	FINAL WT (GM)	STEP H (IN)
6	78	105	18	47	0.5	0.5	0.5	0.5
7	19	20	21	48	0.5	0.5	0.5	0.5
8	21	22	32	49	0.5	0.5	0.5	0.5
15	32	39	42	52	0.5	0.5	0.5	0.5
18	42	48	49	58	0.5	0.5	0.5	0.5
20	52	58	61	61	0.5	0.5	0.5	0.5
21	61	63	62	66	0.5	0.5	0.5	0.5
22	63	66	67	69	0.5	0.5	0.5	0.5
23	66	70	71	72	0.5	0.5	0.5	0.5
24	70	72	73	74	0.5	0.5	0.5	0.5
25	73	74	75	75	0.5	0.5	0.5	0.5
26	74	75	76	76	0.5	0.5	0.5	0.5
27	75	76	77	77	0.5	0.5	0.5	0.5
28	76	77	78	78	0.5	0.5	0.5	0.5
29	77	78	79	79	0.5	0.5	0.5	0.5
30	78	79	80	80	0.5	0.5	0.5	0.5
31	79	80	81	81	0.5	0.5	0.5	0.5
32	80	81	82	82	0.5	0.5	0.5	0.5
33	81	82	83	83	0.5	0.5	0.5	0.5
34	82	83	84	84	0.5	0.5	0.5	0.5
35	83	84	85	85	0.5	0.5	0.5	0.5
36	84	85	86	86	0.5	0.5	0.5	0.5
37	85	86	87	87	0.5	0.5	0.5	0.5
38	86	87	88	88	0.5	0.5	0.5	0.5
39	87	88	89	89	0.5	0.5	0.5	0.5
40	88	89	90	90	0.5	0.5	0.5	0.5
41	89	90	91	91	0.5	0.5	0.5	0.5
42	90	91	92	92	0.5	0.5	0.5	0.5
43	91	92	93	93	0.5	0.5	0.5	0.5
44	92	93	94	94	0.5	0.5	0.5	0.5
45	93	94	95	95	0.5	0.5	0.5	0.5
46	94	95	96	96	0.5	0.5	0.5	0.5
47	95	96	97	97	0.5	0.5	0.5	0.5
48	96	97	98	98	0.5	0.5	0.5	0.5
49	97	98	99	99	0.5	0.5	0.5	0.5
50	98	99	100	100	0.5	0.5	0.5	0.5
51	99	100	101	101	0.5	0.5	0.5	0.5
52	100	101	102	102	0.5	0.5	0.5	0.5
53	101	102	103	103	0.5	0.5	0.5	0.5
54	102	103	104	104	0.5	0.5	0.5	0.5
55	103	104	105	105	0.5	0.5	0.5	0.5
56	104	105	106	106	0.5	0.5	0.5	0.5
57	105	106	107	107	0.5	0.5	0.5	0.5
58	106	107	108	108	0.5	0.5	0.5	0.5
59	107	108	109	109	0.5	0.5	0.5	0.5
60	108	109	110	110	0.5	0.5	0.5	0.5
61	109	110	111	111	0.5	0.5	0.5	0.5
62	110	111	112	112	0.5	0.5	0.5	0.5
63	111	112	113	113	0.5	0.5	0.5	0.5
64	112	113	114	114	0.5	0.5	0.5	0.5
65	113	114	115	115	0.5	0.5	0.5	0.5
66	114	115	116	116	0.5	0.5	0.5	0.5
67	115	116	117	117	0.5	0.5	0.5	0.5
68	116	117	118	118	0.5	0.5	0.5	0.5
69	117	118	119	119	0.5	0.5	0.5	0.5
70	118	119	120	120	0.5	0.5	0.5	0.5
71	119	120	121	121	0.5	0.5	0.5	0.5
72	120	121	122	122	0.5	0.5	0.5	0.5
73	121	122	123	123	0.5	0.5	0.5	0.5
74	122	123	124	124	0.5	0.5	0.5	0.5
75	123	124	125	125	0.5	0.5	0.5	0.5
76	124	125	126	126	0.5	0.5	0.5	0.5
77	125	126	127	127	0.5	0.5	0.5	0.5
78	126	127	128	128	0.5	0.5	0.5	0.5
79	127	128	129	129	0.5	0.5	0.5	0.5
80	128	129	130	130	0.5	0.5	0.5	0.5
81	129	130	131	131	0.5	0.5	0.5	0.5
82	130	131	132	132	0.5	0.5	0.5	0.5
83	131	132	133	133	0.5	0.5	0.5	0.5
84	132	133	134	134	0.5	0.5	0.5	0.5
85	133	134	135	135	0.5	0.5	0.5	0.5
86	134	135	136	136	0.5	0.5	0.5	0.5
87	135	136	137	137	0.5	0.5	0.5	0.5
88	136	137	138	138	0.5	0.5	0.5	0.5
89	137	138	139	139	0.5	0.5	0.5	0.5
90	138	139	140	140	0.5	0.5	0.5	0.5
91	139	140	141	141	0.5	0.5	0.5	0.5
92	140	141	142	142	0.5	0.5	0.5	0.5
93	141	142	143	143	0.5	0.5	0.5	0.5
94	142	143	144	144	0.5	0.5	0.5	0.5
95	143	144	145	145	0.5	0.5	0.5	0.5
96	144	145	146	146	0.5	0.5	0.5	0.5
97	145	146	147	147	0.5	0.5	0.5	0.5
98	146	147	148	148	0.5	0.5	0.5	0.5
99	147	148	149	149	0.5	0.5	0.5	0.5
100	148	149	150	150	0.5	0.5	0.5	0.5







CALCULATED RESULTS

TEST #	WDDOT (LBM/SEC)	CHAMBER T (R)	CHAMBER P (PSIA)	RWT (IN/SEC)	RDE (IN/SEC)	WF (LBM/ SEC)	REST EP (LBM)	FG (LBF)
678	1190	1190	59.6	0.0065	0.0069	0.0183	27.	216.
10	1186	1016	86.1	0.0072	0.0077	0.0239	31.	312.
21	1186	1017	83.6	0.0083	0.0089	0.0283	32.	329.
32	1182	1024	88.6	0.0071	0.0074	0.0293	49.	497.
42	1182	1024	88.6	0.0082	0.0089	0.0293	58.	580.
48	1182	1024	89.6	0.0087	0.0094	0.0308	60.	601.
49	1182	1024	89.6	0.0086	0.0091	0.0308	61.	612.
52	1182	1024	89.6	0.0086	0.0091	0.0308	62.	623.
53	1182	1024	89.6	0.0086	0.0091	0.0308	63.	634.
58	1182	1024	89.6	0.0086	0.0091	0.0308	66.	667.
60	1182	1024	89.6	0.0086	0.0091	0.0308	67.	670.
61	1182	1024	89.6	0.0086	0.0091	0.0308	69.	697.
62	1182	1024	89.6	0.0086	0.0091	0.0308	70.	712.
63	1182	1024	89.6	0.0086	0.0091	0.0308	72.	723.
66	1182	1024	89.6	0.0086	0.0091	0.0308	73.	734.
67	1182	1024	89.6	0.0086	0.0091	0.0308	74.	744.
68	1182	1024	89.6	0.0086	0.0091	0.0308	75.	755.
70	1182	1024	89.6	0.0086	0.0091	0.0308	76.	766.
71	1182	1024	89.6	0.0086	0.0091	0.0308	77.	777.
72	1182	1024	89.6	0.0086	0.0091	0.0308	78.	788.
73	1182	1024	89.6	0.0086	0.0091	0.0308	79.	799.
74	1182	1024	89.6	0.0086	0.0091	0.0308	80.	800.
75	1182	1024	89.6	0.0086	0.0091	0.0308	81.	811.
76	1182	1024	89.6	0.0086	0.0091	0.0308	82.	822.
77	1182	1024	89.6	0.0086	0.0091	0.0308	83.	833.
78	1182	1024	89.6	0.0086	0.0091	0.0308	84.	844.
79	1182	1024	89.6	0.0086	0.0091	0.0308	85.	855.
80	1182	1024	89.6	0.0086	0.0091	0.0308	86.	866.
81	1182	1024	89.6	0.0086	0.0091	0.0308	87.	877.
82	1182	1024	89.6	0.0086	0.0091	0.0308	88.	888.
83	1182	1024	89.6	0.0086	0.0091	0.0308	89.	899.
84	1182	1024	89.6	0.0086	0.0091	0.0308	90.	900.
85	1182	1024	89.6	0.0086	0.0091	0.0308	91.	911.
86	1182	1024	89.6	0.0086	0.0091	0.0308	92.	922.
87	1182	1024	89.6	0.0086	0.0091	0.0308	93.	933.
88	1182	1024	89.6	0.0086	0.0091	0.0308	94.	944.
89	1182	1024	89.6	0.0086	0.0091	0.0308	95.	955.
90	1182	1024	89.6	0.0086	0.0091	0.0308	96.	966.
91	1182	1024	89.6	0.0086	0.0091	0.0308	97.	977.
92	1182	1024	89.6	0.0086	0.0091	0.0308	98.	988.
93	1182	1024	89.6	0.0086	0.0091	0.0308	99.	999.
94	1182	1024	89.6	0.0086	0.0091	0.0308	100.	1000.
95	1182	1024	89.6	0.0086	0.0091	0.0308	101.	1011.
96	1182	1024	89.6	0.0086	0.0091	0.0308	102.	1022.
97	1182	1024	89.6	0.0086	0.0091	0.0308	103.	1033.
98	1182	1024	89.6	0.0086	0.0091	0.0308	104.	1044.
99	1182	1024	89.6	0.0086	0.0091	0.0308	105.	1055.
100	1182	1024	89.6	0.0086	0.0091	0.0308	106.	1066.
101	1182	1024	89.6	0.0086	0.0091	0.0308	107.	1077.
102	1182	1024	89.6	0.0086	0.0091	0.0308	108.	1088.
103	1182	1024	89.6	0.0086	0.0091	0.0308	109.	1099.
104	1182	1024	89.6	0.0086	0.0091	0.0308	110.	1110.
105	1182	1024	89.6	0.0086	0.0091	0.0308	111.	1111.
106	1182	1024	89.6	0.0086	0.0091	0.0308	112.	1112.
107	1182	1024	89.6	0.0086	0.0091	0.0308	113.	1113.
108	1182	1024	89.6	0.0086	0.0091	0.0308	114.	1114.
109	1182	1024	89.6	0.0086	0.0091	0.0308	115.	1115.
110	1182	1024	89.6	0.0086	0.0091	0.0308	116.	1116.
111	1182	1024	89.6	0.0086	0.0091	0.0308	117.	1117.
112	1182	1024	89.6	0.0086	0.0091	0.0308	118.	1118.
113	1182	1024	89.6	0.0086	0.0091	0.0308	119.	1119.
114	1182	1024	89.6	0.0086	0.0091	0.0308	120.	1120.
115	1182	1024	89.6	0.0086	0.0091	0.0308	121.	1121.
116	1182	1024	89.6	0.0086	0.0091	0.0308	122.	1122.
117	1182	1024	89.6	0.0086	0.0091	0.0308	123.	1123.
118	1182	1024	89.6	0.0086	0.0091	0.0308	124.	1124.
119	1182	1024	89.6	0.0086	0.0091	0.0308	125.	1125.
120	1182	1024	89.6	0.0086	0.0091	0.0308	126.	1126.
121	1182	1024	89.6	0.0086	0.0091	0.0308	127.	1127.
122	1182	1024	89.6	0.0086	0.0091	0.0308	128.	1128.
123	1182	1024	89.6	0.0086	0.0091	0.0308	129.	1129.
124	1182	1024	89.6	0.0086	0.0091	0.0308	130.	1130.
125	1182	1024	89.6	0.0086	0.0091	0.0308	131.	1131.
126	1182	1024	89.6	0.0086	0.0091	0.0308	132.	1132.
127	1182	1024	89.6	0.0086	0.0091	0.0308	133.	1133.
128	1182	1024	89.6	0.0086	0.0091	0.0308	134.	1134.
129	1182	1024	89.6	0.0086	0.0091	0.0308	135.	1135.
130	1182	1024	89.6	0.0086	0.0091	0.0308	136.	1136.
131	1182	1024	89.6	0.0086	0.0091	0.0308	137.	1137.
132	1182	1024	89.6	0.0086	0.0091	0.0308	138.	1138.
133	1182	1024	89.6	0.0086	0.0091	0.0308	139.	1139.
134	1182	1024	89.6	0.0086	0.0091	0.0308	140.	1140.
135	1182	1024	89.6	0.0086	0.0091	0.0308	141.	1141.
136	1182	1024	89.6	0.0086	0.0091	0.0308	142.	1142.
137	1182	1024	89.6	0.0086	0.0091	0.0308	143.	1143.
138	1182	1024	89.6	0.0086	0.0091	0.0308	144.	1144.
139	1182	1024	89.6	0.0086	0.0091	0.0308	145.	1145.
140	1182	1024	89.6	0.0086	0.0091	0.0308	146.	1146.
141	1182	1024	89.6	0.0086	0.0091	0.0308	147.	1147.
142	1182	1024	89.6	0.0086	0.0091	0.0308	148.	1148.
143	1182	1024	89.6	0.0086	0.0091	0.0308	149.	1149.
144	1182	1024	89.6	0.0086	0.0091	0.0308	150.	1150.
145	1182	1024	89.6	0.0086	0.0091	0.0308	151.	1151.
146	1182	1024	89.6	0.0086	0.0091	0.0308	152.	1152.
147	1182	1024	89.6	0.0086	0.0091	0.0308	153.	1153.
148	1182	1024	89.6	0.0086	0.0091	0.0308	154.	1154.
149	1182	1024	89.6	0.0086	0.0091	0.0308	155.	1155.
150	1182	1024	89.6	0.0086	0.0091	0.0308	156.	1156.
151	1182	1024	89.6	0.0086	0.0091	0.0308	157.	1157.
152	1182	1024	89.6	0.0086	0.0091	0.0308	158.	1158.
153	1182	1024	89.6	0.0086	0.0091	0.0308	159.	1159.
154	1182	1024	89.6	0.0086	0.0091	0.0308	160.	1160.
155	1182	1024	89.6	0.0086	0.0091	0.0308	161.	1161.
156	1182	1024	89.6	0.0086	0.0091	0.0308	162.	1162.
157	1182	1024	89.6	0.0086	0.0091	0.0308	163.	1163.
158	1182	1024	89.6	0.0086	0.0091	0.0308	164.	1164.
159	1182	1024	89.6	0.0086	0.0091	0.0308	165.	1165.
160	1182	1024	89.6	0.0086	0.0091	0.0308	166.	1166.
161	1182	1024	89.6	0.0086	0.0091	0.0308	167.	1167.
162	1182	1024	89.6	0.0086	0.0091	0.0308	168.	1168.
163	1182	1024	89.6	0.0086	0.0091	0.0308	169.	1169.
164	1182	1024	89.6	0.0086	0.0091	0.0308	170.	1170.
165	1182	1024	89.6	0.0086	0.0091	0.0308	171.	1171.
166	1182	1024	89.6	0.0086	0.0091	0.0308	172.	1172.
167	1182	1024	89.6	0.0086	0.0091	0.0308	173.	1173.
168	1182	1024	89.6	0.0086	0.0091	0.0308	174.	1174.



CALCULATED RESULTS

TEST #	AF	(LBM/SEC. IN2)	GAIR	H/D	XR/D	UPORT (FT/SEC)	ISP (SEC)	SFC
10	10.89	8.915	1.13	0.65	2.00	346.	1457.	2.5
11	15.31	9.79	1.13	0.44	2.15	262.	1147.	2.1
12	14.12	9.95	1.11	0.7	2.04	254.	1521.	2.1
13	14.95	8.68	1.07	1.03	2.07	462.	1745.	2.1
14	17.8	8.91	1.03	1.92	1.88	351.	1931.	2.1
15	15.8	7.79	1.07	1.02	1.89	2227.	1435.	2.1
16	18.2	7.31	1.11	1.11	1.07	2222.	1640.	2.1
17	19.0	7.25	1.11	1.11	1.07	2222.	1647.	2.1
18	19.9	7.0	1.17	1.48	1.02	2222.	1371.	2.1
19	20.1	7.25	1.17	1.70	1.02	2222.	1640.	2.1
20	21.2	7.0	1.17	1.48	1.02	2222.	1371.	2.1
21	23.9	4.8	4.2	4.9	1.02	2222.	1640.	2.1
22	24.8	4.9	5.2	5.2	1.02	2222.	1640.	2.1
23	25.3	5.2	5.8	5.8	1.02	2222.	1640.	2.1
24	25.8	5.2	6.0	6.0	1.02	2222.	1640.	2.1
25	26.2	5.2	6.2	6.2	1.02	2222.	1640.	2.1
26	26.3	5.2	6.3	6.3	1.02	2222.	1640.	2.1
27	26.7	5.2	6.7	6.7	1.02	2222.	1640.	2.1
28	27.0	5.2	6.9	6.9	1.02	2222.	1640.	2.1
29	27.2	5.2	6.9	6.9	1.02	2222.	1640.	2.1
30	27.3	5.2	7.0	7.0	1.02	2222.	1640.	2.1
31	27.4	5.2	7.2	7.2	1.02	2222.	1640.	2.1
32	28.0	5.2	7.4	7.4	1.02	2222.	1640.	2.1
33	28.5	5.2	7.5	7.5	1.02	2222.	1640.	2.1
34	29.0	5.2	7.5	7.5	1.02	2222.	1640.	2.1
35	29.5	5.2	7.5	7.5	1.02	2222.	1640.	2.1
36	30.0	5.2	7.5	7.5	1.02	2222.	1640.	2.1
37	30.5	5.2	7.5	7.5	1.02	2222.	1640.	2.1
38	31.0	5.2	7.5	7.5	1.02	2222.	1640.	2.1
39	31.5	5.2	7.5	7.5	1.02	2222.	1640.	2.1
40	32.0	5.2	7.5	7.5	1.02	2222.	1640.	2.1
41	32.5	5.2	7.5	7.5	1.02	2222.	1640.	2.1
42	33.0	5.2	7.5	7.5	1.02	2222.	1640.	2.1
43	33.5	5.2	7.5	7.5	1.02	2222.	1640.	2.1
44	34.0	5.2	7.5	7.5	1.02	2222.	1640.	2.1
45	34.5	5.2	7.5	7.5	1.02	2222.	1640.	2.1
46	35.0	5.2	7.5	7.5	1.02	2222.	1640.	2.1
47	35.5	5.2	7.5	7.5	1.02	2222.	1640.	2.1
48	36.0	5.2	7.5	7.5	1.02	2222.	1640.	2.1
49	36.5	5.2	7.5	7.5	1.02	2222.	1640.	2.1
50	37.0	5.2	7.5	7.5	1.02	2222.	1640.	2.1
51	37.5	5.2	7.5	7.5	1.02	2222.	1640.	2.1
52	38.0	5.2	7.5	7.5	1.02	2222.	1640.	2.1
53	38.5	5.2	7.5	7.5	1.02	2222.	1640.	2.1
54	39.0	5.2	7.5	7.5	1.02	2222.	1640.	2.1
55	39.5	5.2	7.5	7.5	1.02	2222.	1640.	2.1
56	40.0	5.2	7.5	7.5	1.02	2222.	1640.	2.1
57	40.5	5.2	7.5	7.5	1.02	2222.	1640.	2.1
58	41.0	5.2	7.5	7.5	1.02	2222.	1640.	2.1
59	41.5	5.2	7.5	7.5	1.02	2222.	1640.	2.1
60	42.0	5.2	7.5	7.5	1.02	2222.	1640.	2.1
61	42.5	5.2	7.5	7.5	1.02	2222.	1640.	2.1
62	43.0	5.2	7.5	7.5	1.02	2222.	1640.	2.1
63	43.5	5.2	7.5	7.5	1.02	2222.	1640.	2.1
64	44.0	5.2	7.5	7.5	1.02	2222.	1640.	2.1
65	44.5	5.2	7.5	7.5	1.02	2222.	1640.	2.1
66	45.0	5.2	7.5	7.5	1.02	2222.	1640.	2.1
67	45.5	5.2	7.5	7.5	1.02	2222.	1640.	2.1
68	46.0	5.2	7.5	7.5	1.02	2222.	1640.	2.1
69	46.5	5.2	7.5	7.5	1.02	2222.	1640.	2.1
70	47.0	5.2	7.5	7.5	1.02	2222.	1640.	2.1
71	47.5	5.2	7.5	7.5	1.02	2222.	1640.	2.1
72	48.0	5.2	7.5	7.5	1.02	2222.	1640.	2.1
73	48.5	5.2	7.5	7.5	1.02	2222.	1640.	2.1
74	49.0	5.2	7.5	7.5	1.02	2222.	1640.	2.1
75	49.5	5.2	7.5	7.5	1.02	2222.	1640.	2.1
76	50.0	5.2	7.5	7.5	1.02	2222.	1640.	2.1
77	50.5	5.2	7.5	7.5	1.02	2222.	1640.	2.1
78	51.0	5.2	7.5	7.5	1.02	2222.	1640.	2.1
79	51.5	5.2	7.5	7.5	1.02	2222.	1640.	2.1
80	52.0	5.2	7.5	7.5	1.02	2222.	1640.	2.1
81	52.5	5.2	7.5	7.5	1.02	2222.	1640.	2.1
82	53.0	5.2	7.5	7.5	1.02	2222.	1640.	2.1
83	53.5	5.2	7.5	7.5	1.02	2222.	1640.	2.1
84	54.0	5.2	7.5	7.5	1.02	2222.	1640.	2.1
85	54.5	5.2	7.5	7.5	1.02	2222.	1640.	2.1
86	55.0	5.2	7.5	7.5	1.02	2222.	1640.	2.1
87	55.5	5.2	7.5	7.5	1.02	2222.	1640.	2.1
88	56.0	5.2	7.5	7.5	1.02	2222.	1640.	2.1
89	56.5	5.2	7.5	7.5	1.02	2222.	1640.	2.1
90	57.0	5.2	7.5	7.5	1.02	2222.	1640.	2.1
91	57.5	5.2	7.5	7.5	1.02	2222.	1640.	2.1
92	58.0	5.2	7.5	7.5	1.02	2222.	1640.	2.1
93	58.5	5.2	7.5	7.5	1.02	2222.	1640.	2.1
94	59.0	5.2	7.5	7.5	1.02	2222.	1640.	2.1
95	59.5	5.2	7.5	7.5	1.02	2222.	1640.	2.1
96	60.0	5.2	7.5	7.5	1.02	2222.	1640.	2.1
97	60.5	5.2	7.5	7.5	1.02	2222.	1640.	2.1
98	61.0	5.2	7.5	7.5	1.02	2222.	1640.	2.1
99	61.5	5.2	7.5	7.5	1.02	2222.	1640.	2.1
100	62.0	5.2	7.5	7.5	1.02	2222.	1640.	2.1
101	62.5	5.2	7.5	7.5	1.02	2222.	1640.	2.1
102	63.0	5.2	7.5	7.5	1.02	2222.	1640.	2.1
103	63.5	5.2	7.5	7.5	1.02	2222.	1640.	2.1
104	64.0	5.2	7.5	7.5	1.02	2222.	1640.	2.1
105	64.5	5.2	7.5	7.5	1.02	2222.	1640.	2.1
106	65.0	5.2	7.5	7.5	1.02	2222.	1640.	2.1
107	65.5	5.2	7.5	7.5	1.02	2222.	1640.	2.1
108	66.0	5.2	7.5	7.5	1.02	2222.	1640.	2.1
109	66.5	5.2	7.5	7.5	1.02	2222.	1640.	2.1
110	67.0	5.2	7.5	7.5	1.02	2222.	1640.	2.1
111	67.5	5.2	7.5	7.5	1.02	2222.	1640.	2.1
112	68.0	5.2	7.5	7.5	1.02	2222.	1640.	2.1
113	68.5	5.2	7.5	7.5	1.02	2222.	1640.	2.1
114	69.0	5.2	7.5	7.5	1.02	2222.	1640.	2.1
115	69.5	5.2	7.5	7.5	1.02	2222.	1640.	2.1
116	70.0	5.2	7.5	7.5	1.02	2222.	1640.	2.1
117	70.5	5.2	7.5	7.5	1.02	2222.	1640.	2.1
118	71.0	5.2	7.5	7.5	1.02	2222.	1640.	2.1
119	71.5	5.2	7.5	7.5	1.02	2222.	1640.	2.1
120	72.0	5.2	7.5	7.5	1.02	2222.	1640.	2.1
121	72.5	5.2	7.5	7.5	1.02	2222.	1640.	2.1
122	73.0	5.2	7.5	7.5	1.02	2222.	1640.	2.1
123	73.5	5.2	7.5	7.5	1.02	2222.	1640.	2.1
124	74.0	5.2	7.5	7.5	1.02	2222.	1640.	2.1
125	74.5	5.2	7.5	7.5	1.02	2222.	1640.	2.1
126	75.0	5.2	7.5	7.5	1.02	2222.	1640.	2.1
127	75.5	5.2	7.5	7.5	1.02	2222.	1640.	2.1
128	76.0	5.2	7.5	7.5	1.02	2222.	1640.	2.1
129	76.5	5.2	7.5	7.5	1.02	2222.	1640.	2.1
130	77.0	5.2	7.5	7.5	1.02	2222.	1640.	2.1
131	77.5	5.2	7.5	7.5	1.02	2222.	1640.	2.1
132	78.0	5.2	7.5	7.5	1.02	2222.	1640.	2.1
133	78.5	5.2	7.5	7.5	1.02	2222.	1640.	2.1
134	79.0	5.2	7.5	7.5	1.02	2222.	1640.	2.1
135	79.5	5.2	7.5	7.5	1.02	2222.	1640.	2.1
136	80.0	5.2	7.5	7.5	1.02	2222.	1640.	2.1
137	80.5	5.2	7.5	7.5	1.02	2222.	1640.	2.1
138	81.0	5.2	7.5	7.5	1.02	2222.	1640.	2.1
139	81.5	5.2	7.5	7.5	1.02	2222.	1640.	2.1
140	82.0	5.2	7.5	7.5	1.02	2222.	1640.	2.1
141	82.5	5.2	7.5	7.5	1.02	2222.	1640.	2.1
142	83.0	5.2	7.5	7.5	1.02	2222.	1640.	2.1
143	83.5	5.2	7.5	7.5	1.02	2222.	1640.	2.1
144	84.0	5.2	7.5	7.5	1.02	2222.	1640.	2.1
145	84.5	5.2	7.5	7.5	1.02	2222.	1640.	2.1
146	85.0	5.2	7.5	7.5	1.02	2222.	1640.	2.1
147	85.5	5.2	7.5	7.5	1.02	2222.	1640.	2.1
148	86.0	5.2	7.5	7.5	1.02	2222.	1640.	2.1
149	86.5	5.2	7.5	7.5	1.02	2222.	1640.	2.1
150	87.0	5.2	7.5	7.5	1.02	2222.	1640.	2.1
151	87.5	5.2	7.5	7.5	1.02	2222.	1640.	2.1
152	88.0	5.2	7.5	7.5	1.02	2222.	1640.	2.1
153	88.5	5.2	7.5	7.5	1.02	2222.	1640.	2.1
154	89.0	5.2	7.5	7.5	1.02	2222.	1640.	2.1
155	89.5	5.2	7.5	7.5	1.02	2222.	1640.	2.1
156	90.0	5.2	7.5	7.5	1.02	2222.	1640.	2.1



## CALCULATED RESULTS

TEST	EMPIRICAL EQUATION	RWT (IN/SEC)	PERCENT ERROR
67	0.00638	0.00652	2.2
8105	0.00674	0.006718	6.6
118	0.006839	0.006853	7.3
119	0.006825	0.006816	6.8
220	0.006822	0.006816	3.1
332	0.006856	0.006853	1.5
339	0.006859	0.006853	4.4
442	0.006872	0.006865	4.6
448	0.006872	0.006865	4.6
552	0.006852	0.006853	0.3
558	0.006859	0.006853	0.8
660	0.006906	0.006910	0.2
662	0.006910	0.006910	0.1
663	0.006910	0.006910	0.1
666	0.006910	0.006910	0.1
667	0.006914	0.006914	0.4
669	0.006944	0.006944	7.3
770	0.006944	0.006944	7.3
771	0.006944	0.006944	7.3
772	0.006935	0.006935	6.6
773	0.006935	0.006935	3.1
774	0.006935	0.006935	0.5



## APPENDIX C: NON-SUSTAINING TEST DATA

COMPUTER PROGRAM TO REDUCE DATA FROM SOLID FUEL RAMJET RUNS  
FOR NON-SUSTAINING TESTS.

COMPUTER PROGRAM TO REDUCE DATA FROM SJOLID FUEL RAMJET RUNS  
 FOR NON-SUSTAINING TESTS.  
 BY D. BOAZ

INTEGER TEST, GN  
 DIMENSION AM1(40), GAI(40), RESTEP(40), HD(40),  
 DP(40), BP(40), UPORT(40), TEST(40), T(40),  
 REAL\*8 A(10,7), U(10,7), V(7,33), Y(7,10), X, Y, FXY  
 DATA DSTEP/31.75, 33.503/  
 DATA D/31.62, 5.504/  
 READ(5,502) U(I,1), A(I,1), A(I,2), A(I,3), A(I,5), A(I,6), A(I,7)  
 FORMAT(5,7D10.4)  
 501 CONTINUE  
 DO 504 I=1,7  
 READ(5,505) V(I)  
 505 FORMAT(5D15.0)  
 504 CONTINUE  
 NCTCT=36  
 DO 100 N=1,NTOT  
 READ(5,510) TEST(N), T(N), P(N), DP(N), TIN(N), PC(N)  
 510 FORMAT(12, T10, 6F10.5)  
 100 CONTINUE  
 WRITE(6,600) ///  
 600 FORMAT(16, 605) TAINING TESTS,)  
 605 WRITE(6,610) 'INPUT DATA')  
 610 FORMAT(16, T21, 'TEST', T30, 'T', T38, 'P', T45, 'DP', T53, 'BP',  
 1 T71, 'TEST', T85, 'ORIFICE', T98, 'H', T29, 'F', T62, 'T69, '(PSIG  
 2, T44, '(PSI), T51, '(IN HG), T62, '(F), T79, '(IN), T87  
 3, '(IN), T96, '(IN), '/)  
 DO 200 N=1,NTOT  
 H(N)=(1.5-DSTEP(N)/2.0  
 200 WRITE(6,620) TEST(N), T(N), P(N), DP(N), TIN(N), PC(N), DSTEP(N),  
 1 D(N), H(N)  
 620 FORMAT(16, T78, T22, T29, F5.1, T36, F5.1, T44, F4.1, T52, F5.1, T7  
 1, D=2.46  
 DO 210 N=1,NTOT  
 3BP(N)=BP(N)\*0.491157  
 P(N)=P(N)+BP(N)  
 PC(N)=PC(N)+BP(N)  
 T(N)=T(N)+459.67







## NON-SUSTAINING TESTS



## CALCULATED RESULTS

TEST	H/D	WDDT (LBM/SEC)	RESTEP (LBM/SEC-IN2)	GAIR (LBM/SEC-IN2)	UPORT (FT/SEC)
1	2	359	112	11672	12345
			225	227	226
			29	30	29
			31	33	34
			35	36	35
			37	38	37
			40	41	40
			46	47	46
			50	51	50
			54	55	54
			56	57	56
			57	58	57
			65		



## LIST OF REFERENCES

1. Abbott, D. E. and Kline, J. S., "Experimental Investigation of Subsonic Turbulent Flow Over Single and Double Backward Facing Steps," Journal of Basic Engineering, p. 317, September 1962.
2. Krall, K. M. and Sparrow, E. M., "Turbulent Heat Transfer in the Separated, Reattached, and Redevelopment Regions of a Circular Tube," Journal of Heat Transfer, p.131, February 1966.
3. Netzer, D. W., Hybrid Rocket Internal Ballistics, Naval Postgraduate School, CPIA Publication No. 222. January 1972.
4. Muzzy, R. J., "Applied Hybrid Combustion Theory," A.I.A.A. Paper 72-1143, December 1972.
5. United Technology Center, Sunnyvale, California, Investigation of Fundamental Phenomena in Hybrid Propulsion (U), Vol. I (U), Final Technical Report No. UTC 2097-FR, Contract No. w 64-0659-c, November 1965.
6. Woolridge, C. E., Marxman, G. A., and Kier, R. J., Investigation of Combustion Instability in Hybrid Rockets, Stanford Research Institute, NASA CR 66812.
7. Kumar, R. N. and Stickler, D. B., "Polymer Degradation Theory of Pressure Sensitive Hybrid Combustion," Thirteenth Symposium (International) on Combustion, Combustion Institute, Pittsburgh, p. 1059, 1971.
8. United Technology Center, Sunnyvale, California, Solid Fuel Ramjets, Unpublished Report, TM-36-71-U3, 1971.
9. McCarthy, M. J., Pressure Sensitive Combustion in Hybrid Rockets and Solid Fuel Ramjets, Thesis, Naval Postgraduate School, December 1971.
10. Scurlock, A. C., "Flame Stabilization and Propagation in High Velocity Gas Streams," Meteor Report No. 19, Fuels Research Lab., Massachusetts Institute of Technology, May 1948.
11. Longwell, J. P., "Combustion Problems in Ramjets," Fifth Symposium (International) on Combustion, Combustion in Engines and Combustion Kinetics, Reinhold Publishing Corp., New York, p. 48, 1955.



12. Woodward, E. C., "Applications of Chemical Reactor Theory to Combustion Processes," Symposium on the Literature of the Combustion of Petroleum, Advances in Chemistry Series, No. 20, 1956.
13. Avery, W. H., and Hart, R. W., "Combustor Performance with Instantaneous Mixing," Industrial and Engineering Chemistry, Vol. 45, No. 8, p. 1634, August 1953.
14. Gosman, A. D., Pun, W. M., Runchal, A. K., Spalding, D. B., and Wolfshtein, M., Heat and Mass Transfer in Recirculating Flows, Academic Press, 1969.
15. Spalding, D. B., Gosman, A. D., and Pun, W. M., The Prediction of Two-dimensional Flows, Short Course, Pennsylvania State University, August 1972.
16. Spalding, D. B., "A Two Equation Model of Turbulence," Verein Deutscher Ingenieure, Forschungsheft 549, 1972.
17. Holman, J. P., Experimental Methods for Engineers, McGraw-Hill, 1966.
18. Kustov, Y. A. and Rybanin, S. S., "Effect of Chemical Kinetics on the Burning Rate of a Propellant Slab in a Turbulent Oxidizer Flow," Fizika Goreniya i Vzryva, Vol. 6, No. 1, p. 54, 1970.
19. Hojnacki, J. T. and Schwartzkopf, K. G., "Recent Dump Combustor Developments," Ninth JANNAF Combustion Meeting, CPIA Publication No. 231, Vol. II, p. 357, December 1972.



INITIAL DISTRIBUTION LIST

	No. Copies
1. Defense Documentation Center Cameron Station Alexandria Virginia 22314	2
2. Library, Code 0212 Naval Postgraduate School Monterey, California 93940	2
3. Chairman, Department of Aeronautics Naval Postgraduate School Monterey, California 93940	1
4. Assoc. Professor D.W. Netzer, Code 57Nt Department of Aeronautics Naval Postgraduate School Monterey, California 93940	2
5. Lt. Lowell D. Boaz, USN Department of Aeronautics Naval Postgraduate School Monterey, California 93940	2
6. Lt. C. E. Jones III, USN Department of Aeronautics Naval Postgraduate School Monterey, California 93940	1



## DOCUMENT CONTROL DATA - R &amp; D

(Security classification of title, body of abstract and indexing annotation must be entered when the overall report is classified)

1. ORIGINATING ACTIVITY (Corporate author)		2a. REPORT SECURITY CLASSIFICATION	
Naval Postgraduate School Monterey, California 93940		Unclassified	
3. REPORT TITLE			
Internal Ballistics of Solid Fuel Ramjets			
4. DESCRIPTIVE NOTES (Type of report and, Inclusive dates)			
Master's Thesis; March 1973			
5. AUTHOR(S) (First name, middle initial, last name)			
Lowell David Boaz			
6. REPORT DATE		7a. TOTAL NO. OF PAGES	7b. NO. OF REFS
March 1973		96	19
7a. CONTRACT OR GRANT NO.		9a. ORIGINATOR'S REPORT NUMBER(S)	
b. PROJECT NO.			
c.		9b. OTHER REPORT NO(S) (Any other numbers that may be assigned this report)	
d.			
8. DISTRIBUTION STATEMENT			
Approved for public release; distribution unlimited.			
9. SUPPLEMENTARY NOTES		12. SPONSORING MILITARY ACTIVITY	
		Naval Postgraduate School Monterey, California 93940	
10. ABSTRACT			
<p>An experimental investigation of the internal ballistics of solid fuel ramjets was conducted in order to determine the regression rate of the fuel as a function of chamber pressure, inlet air temperature, and air flux rate, and to model the flow in solid fuel ramjets which use sudden expansion flame-holders at the inlet. In addition, flame stabilization limits were investigated. A computer solution for the non-reacting flow field gave results in good agreement with experiments.</p> <p>Solid fuel ramjets have an average regression rate of the fuel that closely follows the theoretical expression derived for kinetically controlled hybrid rocket combustion. The inlet step-height-to-motor-diameter ratio is the dominant parameter in determining flame stability limits. However, inlet velocity is also an important parameter.</p>			



14 KEY WORDS	LINK A		LINK B		LINK C	
	ROLE	WT	ROLE	WT	ROLE	WT
Ramjet Solid Fuel Recirculating Flow Internal Ballistics						



5 SEP 80

26172

Thesis

144075

B5884 Boaz

c.1 Internal ballistics  
of solid fuel ramjets.

5 SEP 80

26172

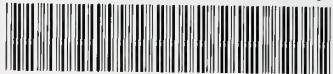
Thesis

144075

B5884 Boaz

c.1 Internal ballistics  
of solid fuel ramjets.

thesB5884  
Internal ballistics of solid fuel ramjet



3 2768 002 07437 9  
DUDLEY KNOX LIBRARY